



Using Low-frequency Sound to Create Non-contact Sensations On and In the Body

Waseem Hassan

waha@di.ku.dk

University of Copenhagen

Denmark

Asier Marzo

asier.marzo@unavarra.es

Universidad Publica de Navarra

Spain

Kasper Hornbæk

kash@di.ku.dk

University of Copenhagen

Denmark

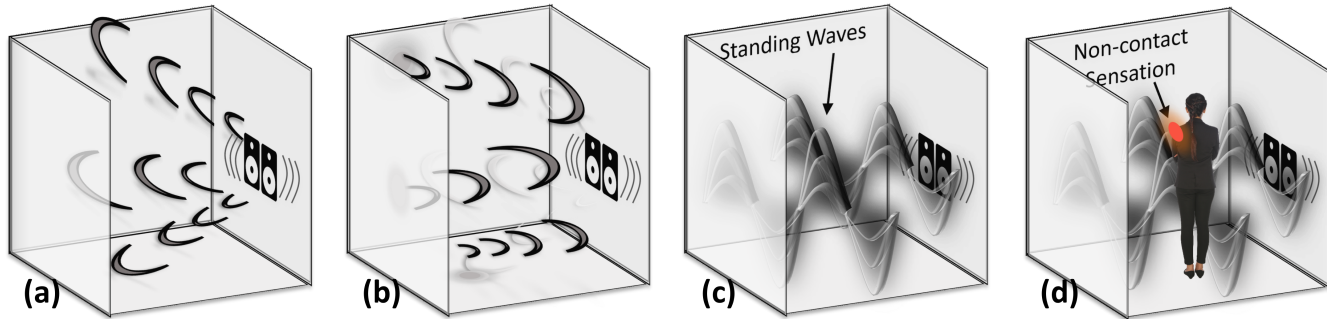


Figure 1: Low-frequency standing waves are used to create non-contact sensations. Panel (a) shows low-frequency sounds emitted from a speaker. Panel (b) shows the sound bouncing off of the room walls. Panel (c) shows how the sound forms standing waves. Panel (d) shows a user perceiving standing waves that produce non-contact sensations on and in the user's body.

ABSTRACT

This paper proposes a method for generating non-contact sensations using low-frequency sound waves without requiring user instrumentation. This method leverages the fundamental acoustic response of a confined space to produce predictable pressure spatial distributions at low frequencies, called modes. These modes can be used to produce sensations either throughout the body, in localized areas of the body, or within the body. We first validate the location and strength of the modes simulated by acoustic modeling. Next, a perceptual study is conducted to show how different frequencies produce qualitatively different sensations across and within the participants' bodies. The low-frequency sound offers a new way of delivering non-contact sensations throughout the body. The results indicate a high accuracy for predicting sensations at specific body locations.

CCS CONCEPTS

- Human-centered computing → Human computer interaction (HCI); Haptic devices; User studies.



This work is licensed under a Creative Commons Attribution International 4.0 License.

CHI '24, May 11–16, 2024, Honolulu, HI, USA

© 2024 Copyright held by the owner/author(s).

ACM ISBN 979-8-4007-0330-0/24/05

<https://doi.org/10.1145/3613904.3642311>

KEYWORDS

Vibrotactile feedback; midair, non-contact haptics; psychophysics; low frequency sounds; room modes.

ACM Reference Format:

Waseem Hassan, Asier Marzo, and Kasper Hornbæk. 2024. Using Low-frequency Sound to Create Non-contact Sensations On and In the Body. In *Proceedings of the CHI Conference on Human Factors in Computing Systems (CHI '24), May 11–16, 2024, Honolulu, HI, USA*. ACM, New York, NY, USA, 22 pages. <https://doi.org/10.1145/3613904.3642311>

1 INTRODUCTION

Haptic devices have evolved significantly over time [19] in an attempt to match the diverse settings in which haptics may be useful. This involves different degrees of mobility [29], precision [49], user engagement [41], or realism [9]. Consequently, the literature contains haptic devices that are grounded [16], wearable [36], encountered-type [31], and mid-air [40].

Numerous review articles published in the past two decades indicate that the focus of most haptic devices is on the hand and forearm [2, 8, 16, 25]. These devices range from grounded force feedback devices to wearable exoskeletons and touch-based tactile devices. Haptic feedback is often delivered through a single-point proxy (or a group of points) [26, 50], which can lead to a reduced sensation of realism and immersion. In an ideal setting, people would prefer to adopt haptic feedback methods that allow them walk-up-and-use or non-personal devices.

Only a few devices overcome the shortcomings of targeting the hand or proxy-based approaches, such as haptic suits [20, 22] or vibrating platforms [11, 12]. They do so at the cost of user comfort

and convenience, imposing wearables that could limit broad acceptability and continuous use. The very need to “wear” the haptic feedback contradicts the ideal of an unobtrusive, natural interaction environment. Thus, innovation in devices that enable non-contact, whole-body sensations is lacking.

We investigate the potential of *low-frequency sounds*, specifically those at or below 200 Hz, to deliver a new dimension of non-contact sensations. Low-frequency sounds are known to generate perceivable vibrations when emitted in a room [32]. This phenomenon, often referred to as “feeling the bass”, is a common experience in scenarios involving powerful sound systems. However, the potential of these vibrations extends beyond mere musical experiences, and control of their spatial resonant modes could target different body parts of the user inside the room.

In a confined space, such as a room, these low-frequency sounds can create standing waves, resulting in a deterministic spatial distribution of acoustic energy. This phenomenon, known as room modes, occurs when the wavelength of the sound matches or is a multiple of the room’s dimensions. Studies have shown that people can perceive these vibrations across various parts of their body, including the chest, abdomen, and thighs [39, 51]. This suggests that low-frequency sounds can be used to create a tactile sensation that engages the entire body, not just the hands or fingers.

The use of low-frequency sounds for delivering sensations has not yet been explored in the field of human-computer interaction (HCI). It is not straightforward to expect that the spatial distribution of these sounds can be meaningfully controlled to deliver sensations. However, the non-contact nature of this approach overcomes the limitations of existing haptic technologies, offering a unique modality of interaction. Specifically, it eliminates the need for wearable or contact-based devices and facilitates a more natural and diverse set of interaction scenarios. While it may be true that haptic feedback does not yet achieve a hyper-realistic level, the implementation of area-based feedback is a step towards more intuitive and natural interaction, especially when compared to the limitations of point-based feedback systems. Furthermore, as mentioned earlier, the haptic feedback is enabled by an acoustically sealed room which might be a limitation in certain use cases.

This paper explores the perceptual effects of these low-frequency sounds and investigates the potential of this method for delivering whole-body sensations. This is achieved by setting up a sealed room and modeling the presence of low-frequency modes in the room, emitted from a subwoofer (Section 3). The model provides the simulation of regions of high and low pressure within the room, which is validated through an experiment (Section 4). In a psychophysical experiment (Section 5), users are first asked to identify perceptual sensations in the presence of the modes (Section 6), report the on or within-body location where the sensations are perceived (Section 7), and later characterize these sensations (Section 8). The understanding developed from the experiment and simulations can lead to generating controlled and meaningful perceptual sensations inside the room and the possible limitations of the system (Section 9).

2 RELATED WORK

Haptic technology has seen significant advancements with a variety of systems to cover a set of increasingly diverse use cases. This

section highlights the research trends in non-contact haptics and whole-body haptics. These trends are crucial to understand the context and potential of the low-frequency sound haptic display being developed.

2.1 Non-Contact Haptic Feedback

Non-contact haptic feedback is a rapidly evolving area that provides tactile sensations in free space without the need for the user to wear or touch any device. This technology has been primarily achieved through the use of focused ultrasound waves, which can create pressure points in the air that the human skin perceives as tactile feedback [6, 30].

Another emerging technology in this field is the use of controlled air vortices [15, 43]. These systems generate donut-shaped air vortices that can travel several meters and deliver a noticeable force upon impact with the skin.

High voltage sparks have been used to induce non-contact tactile sensations on the fingertips [44]. Furthermore, electrostatic haptic displays have also been developed, which use the attractive force between the hair and an electrically charged plate to create a sensation of touch [13, 17].

Non-contact ultrasound devices use multiple ultrasonic emitters that focus at a single point to create a perceivable tactile sensation. The technology has evolved over the last years but some of its major limitations are that the overall tactile feedback is weak, and mainly limited to the palm and fingertips. The air vortex systems provide stronger tactile feedback. However, the time and spatial resolution of the vortices is limited, that is, vortices take dozens of milliseconds to travel to their destination and cannot be aimed accurately. Although the high voltage sparks and electrostatic displays are non-contact, their effective range of action is limited and the stimulation location cannot be controlled. Overall, these non-contact haptic feedback systems often have a confined workspace, weak sensation, or a requirement for close proximity to the display. In contrast, the low-frequency sound haptic display offers a larger workspace and can provide stronger tactile feedback. Moreover, the distance from the sound generator to the user is not a relevant factor, making it a more flexible and versatile solution for providing immersive haptic experiences.

2.2 Whole Body Haptics

Whole-body haptic feedback systems provide tactile sensations to the entire body. These systems often use vibrotactile feedback or pressure/force, delivered through wearable suits or vibrating platforms.

Wearable suits, commonly designed for the torso, come in the form of vests or jackets, with vests offering more size flexibility and jackets covering a larger area including the shoulders. Despite providing feedback over a large surface, these torso-targeted devices have fewer actuators per unit area compared to hand-held wearables and are generally designed for less precise applications since they are worn over clothes. For instance, Tesla Suits provide full-body electro-muscle stimulation to simulate different haptic sensations [46]. Other suits are used for navigation and entertainment [14, 21, 33], and some even provide thermal feedback for added immersion [5]. Additionally, there are specialized haptic vests using shape

memory alloy (SMA) actuators for hugging therapy in children with autism [10].

Vibrating platforms provide underfoot vibrotactile feedback to stimulate the whole body. For instance, a study at the Swedish Museum of Performing Arts explored the role of whole-body vibrations in music composition and perception [11]. Another study noted that such multisensory platforms are accessible and enjoyable for people of various ages [12]. A study investigated the effects of underfoot vibrating platforms in an immersive virtual environment [27], and found that participants felt a higher social presence and displayed more avoidance behavior when a virtual human invaded their personal space.

The use of redirected or encountered-type haptics in VR could be another avenue for whole-body haptics. This approach manipulates sensory perceptions to create illusions of haptic interactions, often reusing the same physical input devices. For example, Azmandian et al. [4] demonstrated the feasibility of redirecting hand-based haptic sensations to simulate whole-body interactions in VR, significantly enhancing the realism of virtual experiences. In the same vein, another study proposes using proxies shaped as geometric primitives to simulate touch feedback in VR scenes, enhancing the user's tactile experience through hand redirection and gaze analysis [7]. Researchers have also used moving robots [34] or drones [1, 3] as haptic interfaces to provide haptic sensations at the time of interaction.

The low-frequency sound haptic display developed in this study can be considered a form of whole-body feedback. However, instead of using contact mechanical vibrations or thermal changes, it uses sound waves to stimulate the sense of touch. This approach offers a unique advantage as it does not require the user to wear or touch any equipment or physical prop.

3 SIMULATING MODAL RESPONSE OF A CONFINED SPACE

Low-frequency sounds are characterized by their long wavelengths (several meters) and their ability to diffract or bend around obstacles more easily than higher-frequency sounds. In this section, we simulate the modal response of a room to low-frequency sounds using the Helmholtz equation of wave propagation. The simulation is carried out using Finite Element Analysis (FEA).

3.1 Helmholtz Equation for Modeling Standing Waves

In acoustics, particularly within enclosed spaces such as rooms, the behavior of sound waves is complex. One of the key phenomena that occur is the formation of standing waves, also known as room modes. These are the result of sound waves reflecting off the walls, ceiling, and floor of the room, and then interfering with each other.

The frequencies at which these modes occur are determined by the dimensions of the room and the speed of sound. Specifically, each mode of the standing wave is associated with a unique frequency, which can be calculated using the following equation:

$$f_{pqr} = \frac{c}{2} \sqrt{\left(\frac{p}{L_x}\right)^2 + \left(\frac{q}{L_y}\right)^2 + \left(\frac{r}{L_z}\right)^2} \quad (1)$$

In this equation, f_{pqr} is the frequency of the mode with indices p , q , and r ; c is the speed of sound, and L_x , L_y , and L_z are the lengths of the room in the x , y , and z directions, respectively. The mode numbers p , q , and r represent the number of half-wavelengths that fit within the lengths L_x , L_y , and L_z in the respective directions.

Room modes, defined by their interaction with room dimensions, include axial (sound waves reflecting off two parallel surfaces), tangential (involving four surfaces), and oblique (engaging all six surfaces). Axial modes exert the highest pressure, followed by the weaker tangential and the weakest oblique modes.

The current study uses the Helmholtz equation to model the behavior of these standing waves. The Helmholtz equation describes how pressure waves propagate in a medium. Its general form in cartesian coordinates is represented as:

$$\nabla^2 \phi + k^2 \phi = 0 \quad (2)$$

where ϕ represents the scalar field, k is the wavenumber (related to the frequency of the wave and the speed of sound), and ∇^2 is the Laplacian operator that represents the divergence of the gradient of ϕ . The general form of the solution to the 3D Helmholtz equation in free space is given by:

$$\phi(x, y, z) = Ae^{i(k_x x + k_y y + k_z z)} \quad (3)$$

where A is the amplitude of the wave, and k_x , k_y , and k_z are the components of the wavevector $\mathbf{k} = k_x \mathbf{i} + k_y \mathbf{j} + k_z \mathbf{k}$. This solution represents a wave traveling in the direction of the wavevector \mathbf{k} , with a frequency determined by the magnitude of \mathbf{k} .

A solution of the Helmholtz equation within a bounded domain is required in the current case, specifically a rectangular room. We apply the Neumann boundary condition, which specifies that the pressure gradient is zero on the walls of the room, simulating sound-hard surfaces:

$$\frac{\partial \phi(x, y, z)}{\partial n} = 0, \quad \text{for } (x, y, z) \in \partial\Omega \quad (4)$$

where $\partial\Omega$ represents the boundary of the domain (in this case, the walls of the room), and $\phi(x, y, z)$ is the pressure amplitude at a point (x, y, z) in the room. In the current context, the Neumann boundary condition corresponds to the assumption of sound-hard surfaces at the room walls. This assumption is reasonable for low-frequency sounds, which are known to reflect almost completely off surfaces like walls.

Upon re-arranging the Helmholtz equation (2), we can represent it in the form of a standard eigenvalue problem:

$$(-\nabla^2)\hat{p} = k^2 \hat{p} \quad (5)$$

where the scalar field ϕ is replaced by \hat{p} to represent the pressure field. The eigenvalues (k^2) represent the square of the wavenumber ($k = \frac{2\pi f}{c}$, with f being the frequency in Hz and c being the speed of sound in m/s) and the corresponding eigenfunctions (\hat{p}) of the Laplacian operator represent the mode shapes.

The solution in Equation 3 represents a wave traveling in an infinite domain without any boundaries. However, the Neumann boundary condition restricts it to a confined room. A standing wave in one dimension can be represented by a cosine or sine function. Therefore, the solution in Equation 3 can now be written as,

$$\hat{p}(x, y, z) = A \cos(k_x x) \cos(k_y y) \cos(k_z z) \quad (6)$$

The eigenvalues in this problem are k_x^2 , k_y^2 , and k_z^2 , and the corresponding eigenfunctions are $\cos(k_x x)$, $\cos(k_y y)$, and $\cos(k_z z)$, respectively. Each factor $\cos(k_i x_i)$ (where $i \in \{x, y, z\}$) can be seen as an eigenfunction of the 1D Laplacian operator $-d^2/dx_i^2$, with the corresponding eigenvalue being k_i^2 . The overall solution $\hat{p}(x, y, z)$ is then an eigenfunction of the 3D Laplacian operator $-\nabla^2$, with the corresponding eigenvalue being $k^2 = k_x^2 + k_y^2 + k_z^2$, which represents the square of the wavenumber of the 3D mode.

These eigenvalues and eigenfunctions of the problem are determined by the dimensions of the room and the boundary conditions. The values of k_x , k_y , and k_z represent the number of half-wavelengths that fit along the x, y, and z dimensions of the room, respectively. Each combination of k_x , k_y , and k_z values represents a different mode of vibration of the room, and the frequency of each mode can be calculated using equation 1.

We investigated the influence of a sinusoidal source term on the modal responses of the room. The modified Helmholtz equation with a source term is expressed as:

$$\nabla^2 \phi + k^2 \phi = S(x, y, z) \quad (7)$$

where $S(x, y, z) = A \sin(2\pi f t)$, with A being the amplitude and f being the frequency of the source term. After solving the equation with the source term, we observed that its inclusion did not alter the modal patterns or frequencies of the room, even when the source frequency was matched with the room's natural frequencies. This suggests that the modes of the room, which are an intrinsic property of the room's dimensions, are not easily perturbed by the introduction of a local source. As such, the source term was ultimately omitted from the final analyses, as its presence did not contribute to the room's modal characteristics.

3.2 FEA Solution of the Helmholtz Equation

The simulations were carried out for a room with dimensions $L_x = 1.7m$, $L_y = 2.18m$, and $L_z = 2.12m$, representing the length, width, and height, respectively. It was modeled using 3D solid primitives. A 3D mesh was generated over the room volume with a voxel size of approximately $0.001m^3$. The mesh quality significantly influences the accuracy of the simulation, and the chosen mesh size provided a balance between computational feasibility and sufficient spatial resolution for the low-frequency modes of interest.

The Helmholtz equation (5) was implemented in the Wolfram Language executed on a Jupyter notebook using the built-in FEM functionality. Linear basis functions were used to represent the solution over each element of the mesh, leading to a system of linear equations that could be solved to obtain the pressure distribution in the room. All the modes with frequencies up to 200 Hz were considered, corresponding to the low-frequency sounds of interest for haptic feedback applications. A total of 14 modes were detected (see Table 1).

After obtaining the mode frequencies and mode shapes, the results were visualized using 3D density plots, as shown in Fig. 2. This involved converting the eigenvectors to pressure distributions over the room volume and plotting them. This provided the simulated

	Mode Type	Mode Frequency (Hz)	p	q	r
1	Axial	78.05	0	1	0
2	Axial	80.26	0	0	1
3	Axial	100.09	1	0	0
4	Tangential	111.95	0	1	1
5	Tangential	126.92	1	1	0
6	Tangential	128.29	1	0	1
7	Oblique	150.17	1	1	1
8	Axial	156.1	0	2	0
9	Axial	160.51	0	0	2
10	Tangential	175.53	0	2	1
11	Tangential	178.49	0	1	2
12	Tangential	185.44	1	2	0
13	Tangential	189.17	1	0	2
14	Axial	200.18	2	0	0

Table 1: A list of the modes calculated from the given dimensions of the room along with their corresponding mode indices (p, q, r) values and the type of mode. The type of mode is determined based on which indices are nonzero. Axial modes have one nonzero index, tangential modes have two, and oblique modes have all three indices nonzero.

results for the spatial distribution of pressure fields in the room, indicating areas of high and low pressure.

4 QUANTITATIVE CHARACTERIZATION

The goal of the quantitative analysis was to compare the simulated pressure fields, shown in Fig. 2, with the actual measurements taken within the room. This comparison was carried out to validate the simulation results.

4.1 Materials

4.1.1 Room Specifications. The experiment was conducted in a controlled environment, a room measuring $1.7 \times 2.18 \times 2.12 m^3$. The size of the room is not a critical factor, other sizes can be used to generate the same effect. All sides of the room were covered with MDF (medium-density fiberboard) of 26 mm thickness, ensuring a consistent and isolated acoustic environment. MDF was used to increase the reflection of sound waves at the boundaries. The dimensions of the room are provided in Fig. 3.

4.1.2 Signal Generation and Recording. All low-frequency sounds (modal frequencies) were pure Sine waves generated using a laptop computer (ASUS Zephyrus G15) running MATLAB R2023a. To prevent transient disturbances and ensure a smooth sound profile, we linearly faded the beginnings, and endings of these signals (350 ms at both ends). The amplitude of the signal was kept at 5 % (113 dB-SPL) of the line level throughout the recordings and subsequent user studies to ensure that the sound did not cause discomfort to the users. Each signal was played for a duration of five seconds.

The sound was produced using a commercially available subwoofer – SB 4000 by SVS – which comes with a 1200-watt class D amplifier (up to 4200 watts at peak capacity). It is capable of producing a maximum amplitude of 126.8 dB SPL. The frequency signals

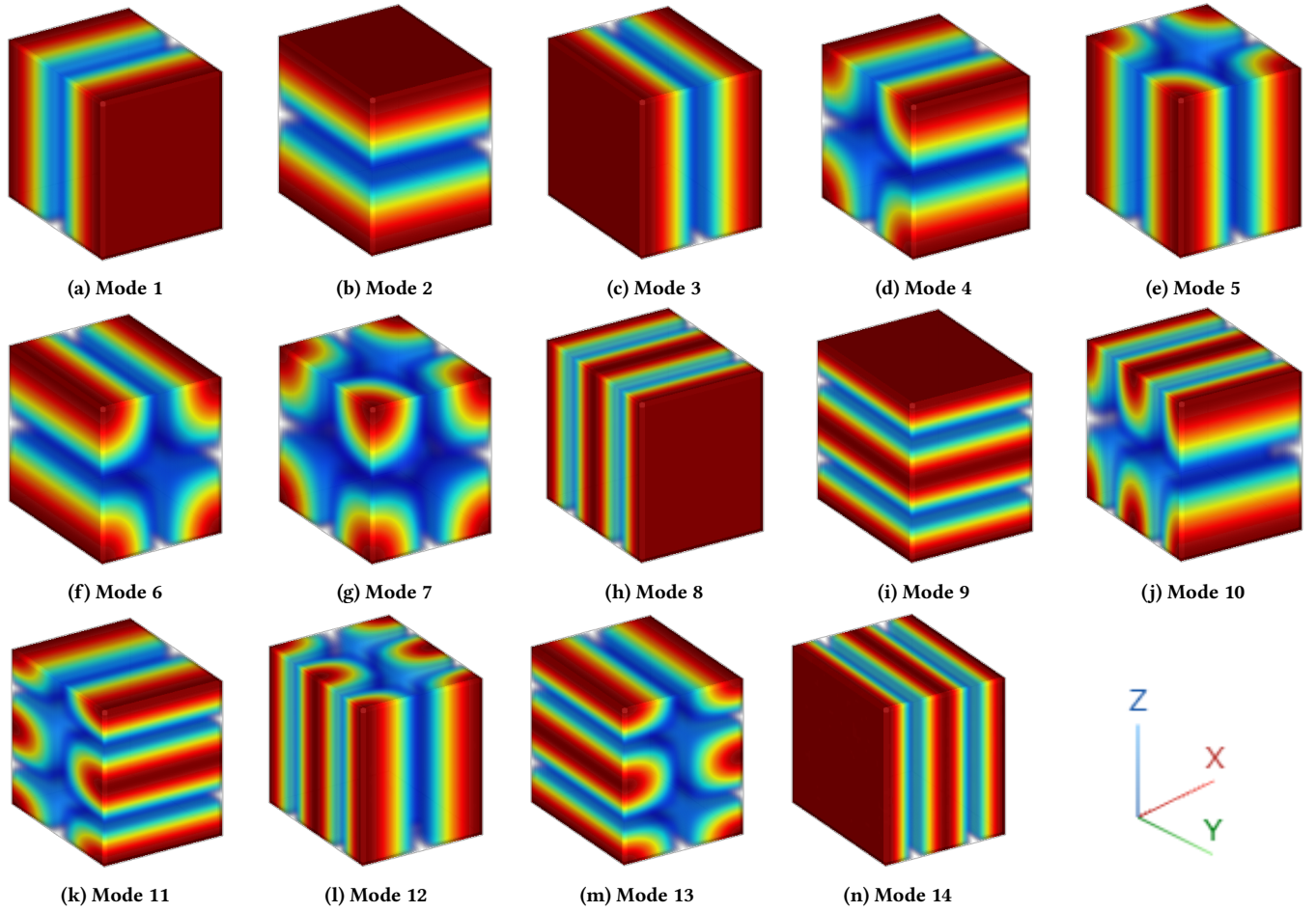


Figure 2: The first 14 modes of the simulated room. Each subfigure shows the pressure distribution of the standing sound waves in the room for the corresponding frequency of the mode. The pressure values for each mode are independently normalized to aid visualization. The red color indicates regions of highest pressure and the blue areas indicate lowest pressure. The intensity of the pressure fields can be seen in Fig. 6

were relayed to the subwoofer through a pre-amplifier (Scarlett 6i by Focusrite).

Measurements of the pressure field were taken using the Blue Yeti condenser microphone set to Omni mode, ensuring accurate digital data collection.

4.2 Methodology

The simulation results in Fig. 2 show the pressure in different areas within the room. In order to get recordings across different pressure zones, we selected a total of 15 points across the xy plane, combined with three different heights in the z plane, resulting in a total of 45 points in the room. The 45 points were selected so that some of the points coincide with high pressure areas of most modes, and some points coincide with low pressure areas. The Cartesian coordinates of the selected locations were $x = \{0.1, 0.9, 1.6\}$, $y = \{0.1, 0.5, 1.0, 1.5, 2.1\}$, $z = \{0.3, 1.0, 1.7\}$.

The data from the microphone were transferred to the laptop computer for Fourier analysis. To ensure consistency and account

for any minor fluctuations, sound at each location was measured two times.

4.3 Data Analysis

The SB 4000 subwoofer's maximum output of 126.8 dB was used as a reference. The simulation pressure values were first normalized and then scaled by 126.8 dB. The volume of the signal was taken into account by subtracting 13 dB (5 % corresponds to 13 dB) from all the simulation values. For data visualization purposes, the simulated and recorded values were normalized to be between zero and one.

Fast Fourier transform (FFT) analysis was performed on the recorded signals to calculate the magnitudes of the associated frequencies. The magnitudes of the recorded and simulated pressures were compared using Mean Absolute Error (MAE). The spatial gradients of these fields were also evaluated to capture trends in pressure variations. The rate of change or the gradient of pressure, from areas of high to low pressure, was examined in both the simulated and recorded environments.

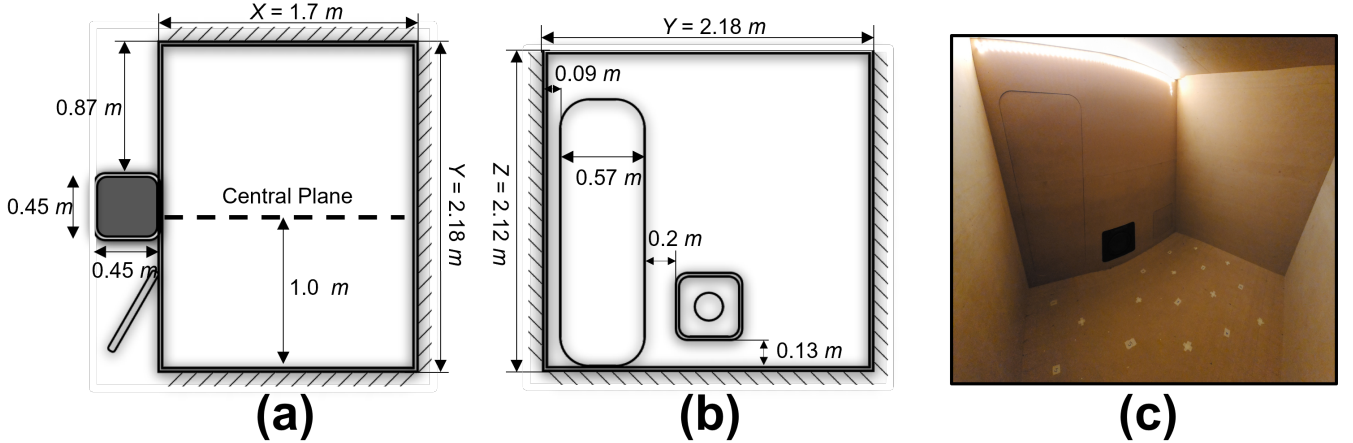


Figure 3: The top view (a), side view (b), and real experimental room (c). Dimensions are in meters.

Instead of a direct point-to-point comparison between simulated and recorded values, we used a volumetric approach that considers the spatial context around each measurement location. For each recorded point, the corresponding location in the simulated data was identified. Around this simulated data point, a cuboid of dimensions 0.1 m^3 was defined. The average pressure value within this cuboid was then calculated and compared to the recorded value at the corresponding location. This methodology ensures a more robust comparison by accounting for slight positional deviations and data noise, thereby mitigating the impact of localized anomalies.

4.4 Results

The presentation of results from the quantitative experiment is divided into two subsections. First, the MAE for all 14 modes is reported. Second, a one-to-one comparison of six selected modes is presented to highlight the variations in pressure fields in the simulated and recorded values. The analysis of these findings serves as the foundation for the subsequent perceptual study.

4.4.1 Mean Absolute Error. The MAE between the recorded and simulated pressure values for each mode are presented in Fig. 4. Each bar in the graph represents the averaged MAE of 45 locations in the room and the error bars indicate the standard deviation in MAE across these locations. The MAE for the 14 modes ranges from 13.5 % for mode 2 to 39.8 % for mode 11. The magnitude of this error is further explained in Fig. 13 provided in the Appendix.

4.4.2 Pressure Distribution Trends. Figure 5 shows a one-to-one comparison of simulated and recorded values for six selected modes (all values are provided in the appendix in Table 4); two modes (mode 2 and 8) with relatively lower MAE, three modes (mode 4, 6, 11, 13) with highest MAE, and one mode (mode 6) with intermediate MAE. The plots in Fig. 5 are marked with black and red dots at the location of comparison. The black dots indicate simulated pressure values that are higher than 80 % of the maximum, while the red dots mark the remaining values. Most of the black dots in recorded values are similar in pressure magnitude to the simulated values. This is a significant result for the current study since these are areas where

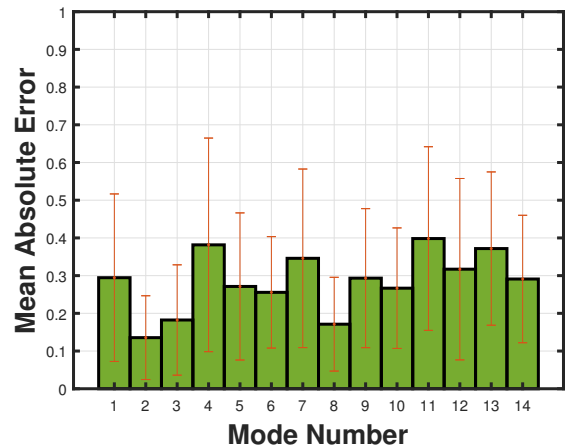


Figure 4: The mean absolute error between the recorded values and simulation values at 45 locations in the room. The error bars show the standard deviation of error across the 45 locations. The y-axis shows the error values normalized between 0 and 1.

most of the sensations are perceived by the users. Comparison for modes 2 and 8 show that the recorded values largely follow the same spatial gradients as simulated values. The results for mode 6 show that the overall gradient or trend in pressure changes was largely consistent between the two, however, the rate of change differed. The graphs for modes 4, 11, and 13 indicate a significant difference in the slopes of the simulated and recorded pressure values. Despite the significant MAE for these modes, the areas of high simulated pressure are still consistent with the recordings. If the error in these comparisons is less than the JND, which ranges from 17% to 21% [38] for the relevant vibration frequencies, then the accuracy is acceptable for this study.

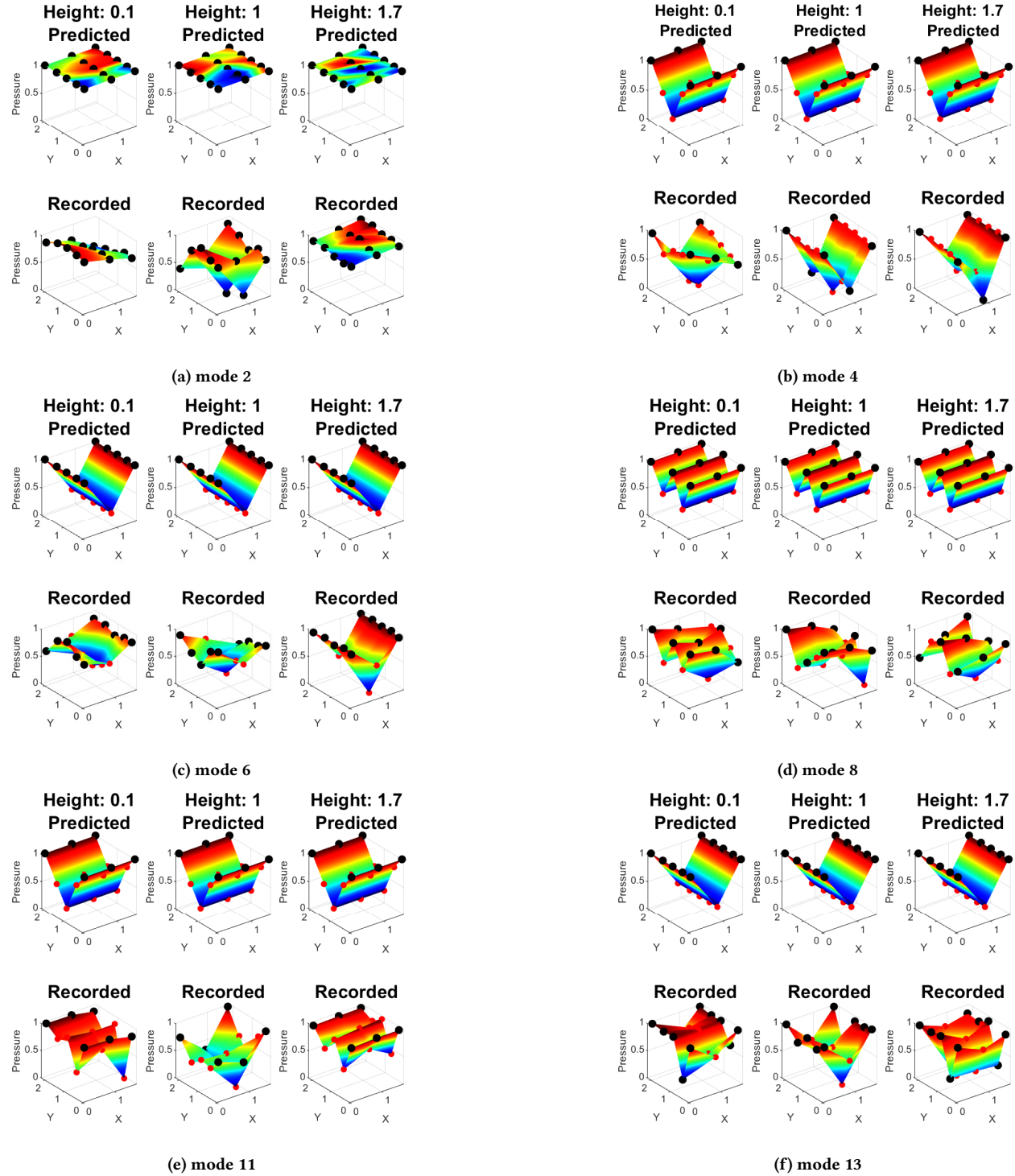


Figure 5: Comparison of simulated and recorded pressure values across 45 distinct locations within the room, presented at three different heights for six representative modes. Black dots denote simulated pressure values that exceed 80 % of the maximum, with corresponding recorded pressure values highlighted at the same locations. The focus is primarily on these high-pressure regions, marked by black dots, as they are of particular interest for this study. Red dots represent the remaining pressure values.

4.4.3 Discussion. While the quantitative differences in the slopes of the pressure fields are noteworthy, it is important to consider the implications for human perception. Human perception is generally more sensitive to changes in pressure rather than the absolute magnitude of sound pressure levels. Therefore, the directional trends or gradients in pressure changes, rather than the exact dB values, may carry greater significance when evaluating their perceptual impact. It is also necessary to emphasize that the primary interest of this study is in areas of high pressure. This is based on the assumption that these regions are more likely to evoke sensations. Keeping these results in mind, the experiment in Sect. 5 was conducted in areas of high simulated pressure.

5 PERCEPTUAL CHARACTERIZATION

The aim of the following experiment is to identify whether participants can perceive the sensations, where on their bodies they perceive them, and how they describe the sensations. This is particularly important for low-frequency sound-based feedback, as the perception of these sounds can be influenced by various factors, including the amplitude and frequency of the sound, and the size and shape of the space.

5.1 Experimental Design

The experiment was a within-subject design, that is, every participant received all the stimuli. For each trial participants were located in one of the regions outlined in Fig. 6. There were two locations for every mode. At all locations, the participants were facing an imaginary central plane of the room (at $y = 1.0$, shown in Fig. 3) while staying perpendicular to the y -axis. The emitter plane of the speaker was at $y = 0$, and therefore always on the side of the participants. The location of the speaker is shown in Fig. 3. The orientation of the participant was kept constant in order to minimize any biases that may arise due to the perceptual threshold differences in the front and back sides of humans. In case any differences did emerge, they would be due to the pressure distribution and not due to the orientation of the participants.

5.1.1 Stimuli. The stimuli used in this experiment were designed based on the modal pressure fields shown in Fig. 2. These fields were systematically analyzed to identify the regions exhibiting the highest pressure. A region was defined as a cuboid with dimensions $0.5m \times 0.5m \times 2.12m$, in line with the average width and depth of a human being. The height of the cuboid was fixed from floor to ceiling to minimize potential bias that might arise due to variations in the height of participants. The whole room was divided into non-overlapping cuboids, and the pressure due to modal frequencies was integrated over the region of the cuboid. Two regions with the highest cumulative pressure were selected for each mode resulting in a total of $(2 \times 14) = 28$ regions. The regions for each of the modes are shown in Fig. 6.

For instance, Fig. 6a shows the two experimental locations for mode 1. The participant is moved to one of these locations before mode 1 is played. Figure 6o (Fig. 6, subfigure o) shows the ten locations which is achieved by aggregating of the locations for all 14 modes. The two locations for mode 1 correspond to locations 4 and 8 in this figure. Each location in Fig. 6o represents experimental

Location	Modes
1	5, 7, 12
2	3, 6, 12, 13
3	3, 5, 6, 7, 13
4	1, 4, 11
5	2, 14
6	8, 10
7	9, 14
8	1, 4, 11
9	2, 8, 10
10	9

Table 2: The list of modes played at the different experimental locations. The experimental locations in the room are shown in Fig. 6o

locations for a subset of the 14 modes. These are detailed in Table 2 for convenience.

5.1.2 Apparatus. The experiment was conducted in an enclosed room measuring $1.7m \times 2.18m \times 2.12m$. The detailed dimensions of the room and the real experimental room are provided in Fig. 3. The apparatus utilized in this experiment was the same as that described in Section 4.1. Participants remained standing throughout the experiment. To focus on the sense of touch and minimize auditory influences, participants were provided with earplugs.

5.2 Participants

A total of 14 participants took part in this experiment. Their mean age was 27.5 years (ranging from 22 to 41), four self-reported as female, and 10 as male. The mean height of the participants was 172.8 cm with a standard deviation of 5.3 cm, and the maximum height was 183 cm. The experiment took 45 minutes on average to complete excluding breaks. They reported no disabilities that would affect the outcome of the experiment. Informed consent was granted by all participants before the experiment. The participants were rewarded with 25 \$ worth of gifts after the experiment.

5.3 Procedure

Written and verbal explanations about the experimental procedure were provided to the participants before the experiment. A reference stimulus containing all 14 modes was played as training before the experiment. This was done so that the participants could establish a mental scale of all the intensities in the experiment.

For the experiment, participants were positioned within one of the predefined regions outlined in Fig. 6. Then, the frequency associated with the specific region was played through a subwoofer. Each stimulus lasted for 5 seconds. Participants were permitted to request multiple playbacks of the stimulus.

After each stimulus, participants provided three kinds of feedback. First, they rated the intensity of the sensation. The intensity rating was conducted on a Likert scale of one to seven. The Likert scale was anchored at the lower end (1) by “Very Mild” and at the higher end (7) by “Very Intense”. Second, they provided detailed verbal descriptions of the sensations. They were allowed to report no sensation. The intensity value and the verbal descriptions were

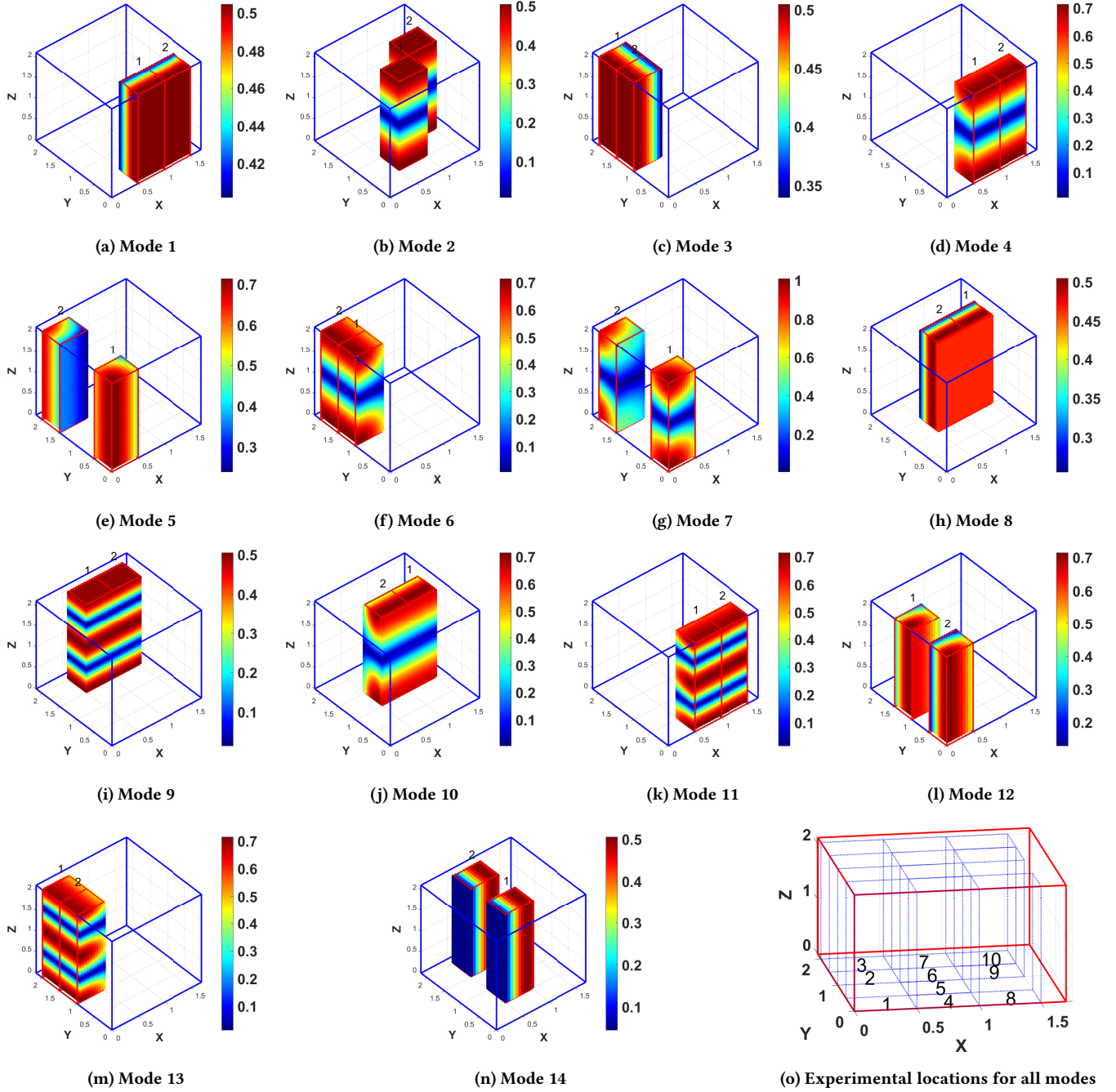


Figure 6: The two regions of highest pressure for the first 14 modes in an enclosed room. The regions are non-overlapping and $0.5\text{m} \times 0.5\text{m} \times 2.12\text{m}$ in size. Subfigure o shows the ten locations where all the 28 (14×2) experimental trials were conducted. This is achieved by combining the two locations shown for each mode in subfigures a to n. The minimum distance between the center of high and low pressure area is 0.5 m.

typed into a smartphone. Third, participants identified and marked any area(s) on a chart of the human body where they experienced sensations. There was no time limit for responding.

5.4 Data Analysis

The perceptual characterization experiment generated three types of data, namely, sensation intensity, verbal sensation description, and the on-body location of sensations. These data were analyzed

to provide insights into how different frequency modes and room locations affected participants' sensory experiences.

5.4.1 Sensation Intensity. The aim of recording intensity data was to uncover whether the participants perceived the sensations at all. And if the sensations were perceived, whether the modes or locations had any effect on the intensity. It was expected that locations would not have any significant effect on intensity as all locations were the ones where high pressure was predicted. Modes, on the other hand, might influence intensity since higher-frequency sounds carry more energy at the same amplitude, however, the set of frequencies (57Hz to 200Hz) in this study is not broad enough to incur significant changes in sound energy.

Before statistical tests, the distribution of the intensity data was analyzed. Based on this distribution, parametric or non-parametric tests were performed. The distribution of data was determined using the Shapiro-Wilk test. The intensity data revealed a non-normal distribution of the data, therefore, non-parametric tests such as the Kruskal-Wallis H and Friedman tests were used to evaluate the effect of frequency modes on intensity ratings. Post-hoc comparisons using the Bonferroni correction method were also conducted to identify specific frequency modes or locations that differ significantly in terms of intensity. The interaction effects of frequency and location were analyzed after aligning the data using the Aligned Rank Transform.

5.4.2 On-Body Sensation Mapping. The data analyzed in this subsection were the ones reported by participants where they highlighted sensation locations on or within their bodies. It was then digitized by marking the same silhouette in a computer at the corresponding locations. The data were also normalized for each mode independently, while the front and back sides of a particular mode were normalized using the same normalization factor.

5.4.3 Verbal Sensation Descriptions. Participants' verbal descriptions of the sensations were subjected to a thematic analysis. The descriptors were categorized and counted to identify recurring themes and overarching patterns in sensory perception. This analysis aimed to assess the consistency between simulated pressure fields and participants' experiences, as well as to identify emergent perceptual properties.

6 RESULTS: SENSATION INTENSITY

Figure 7 shows the histogram of intensity ratings. It shows that a majority of the responses were between three and six which shows that most participants felt intermediate to high intensity. Only 8.1 % of the participants perceived a rating of one which is categorized as "very mild". This result suggests that the sensations were successfully perceived most of the time.

The data from all participants was grouped together for each of the modes for statistical testing, shown in Fig. 8a. The Kruskal-Wallis test with $H(13) = 26.7758$, $p = 0.0134$ and Friedman test with $X^2(13) = 46.36$, $p < 0.001$, were significant. Post-hoc comparisons identified that only Modes 8 and 13 had statistically different intensity ratings.

Similarly, the effect of location on sensations was tested by grouping data from all modes at the 10 locations (as shown in Fig. 6o) in the experiment. The intensity ratings are provided in Fig. 8b. The

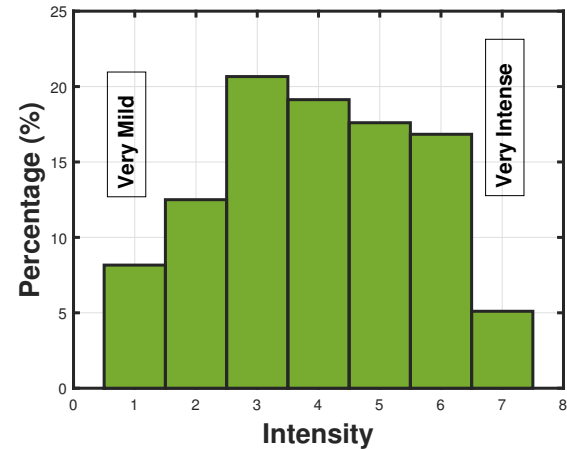


Figure 7: The histogram of intensity ratings showing the percentage times each of the intensity values was recorded by participants.

Kruskal-Wallis h test p -value = 0.0733, and the Friedman test p = 0.12, were not significant.

A two-factor unbalanced ANOVA was conducted to examine the combined effect of mode and location on the intensity ratings. The data were aligned using the Aligned Rank Transform (ART) for two-way factorial analyses. The ANOVA analysis on the aligned data showed that the interaction term was not significant ($p = 0.1795$).

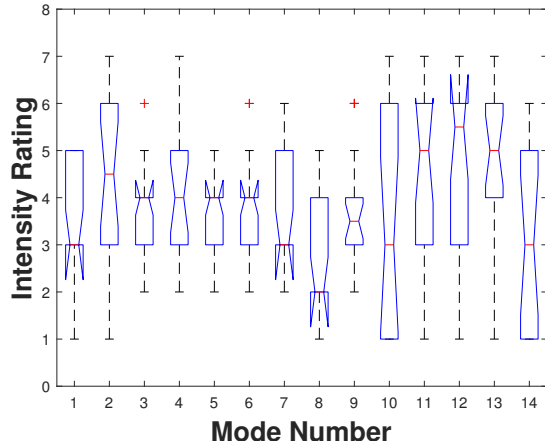
6.1 Discussion

We found a statistically significant impact of frequency modes on intensity ratings. However, post-hoc analysis could not pinpoint many specific pairs of modes that were statistically different. Therefore, while frequency matters, it might not be the sole determinant of intensity. The two-factor unbalanced ANOVA without interaction effects suggests that location does not significantly influence intensity ratings. This result was expected as the locations were nearly identical from a mode point of view, with both locations being those with the highest simulated pressure.

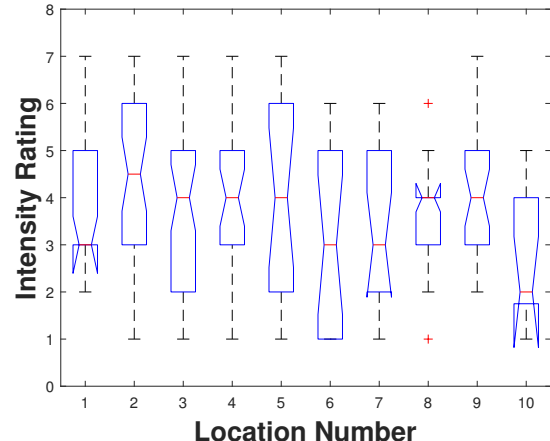
The absence of significant differences in intensity ratings across most modes suggests a few key points. First, participants did not seem to utilize variations in stimulus intensity as a mechanism to differentiate sensations at different body locations. This leads to the conclusion that the role of intensity as a differentiating factor is minimal at best. Second, the uniformity in intensity ratings across different modes implies that most participants perceived the stimuli to be similarly intense, regardless of their frequency or location. This further suggests that other factors, possibly including the quality or type of sensation, may play a more critical role in differentiating experiences across body locations.

7 RESULTS: ON BODY SENSATIONS

The on-body location data were analyzed in three steps of increasing detail. First, the most reported locations were the feet, followed by



(a) Intensity ratings of sensations with respect to modes



(b) Intensity ratings of sensations with respect to location

Figure 8: The intensity ratings for each of the 14 modes used in this experiment. Intensity ratings for the two experimental locations of each mode are combined in (1), while intensity ratings for all modes in a given location are combined in (2).

the lower legs, and upper chest area. Second, a segmented comparison with the simulation results showed that the reported on-body sensations followed the simulation results with a mismatch of 10.67 %. Third, a comparison of the reported sensations and simulation results for similar modes is provided, highlighting the trends and explaining the divergences in participant responses.

7.1 A holistic representation

This subsection presents an analysis of the sensation locations reported by participants, shown in Figure 9. Predominantly, sensations were felt on the feet's front and the chest area within the trunk region. While the entire body silhouette shows reported sensations, the front was notably more reported than the back. This discrepancy may stem from the back's lower perception threshold, participants' frontal focus, and experimental setup directing the front side towards the room's center, as elaborated in Section 7.3. The reasons behind the front-back sensation mismatch require further controlled investigation.

7.2 Segmental Comparison

The aim of this analysis was to numerically evaluate the reported on-body locations against the simulation results. The reported locations from the perceptual study and the corresponding data from simulations are provided in Fig. 10 and Fig. 11, respectively. Table 3 shows the accuracy of the reported sensations when compared with the simulations. This comparison was carried out only for the front side of the body as it was reported significantly more and showed the most diversity in locations. The lack of sensations on the back is discussed in Sect. 7.3. The details of the comparison are provided below.

7.2.1 Method. The on-body location data and simulated pressure regions were divided into five segments of equal height. The purpose of this segmentation was to allow for a localized comparison. The modes with the maximum number of transitions according to

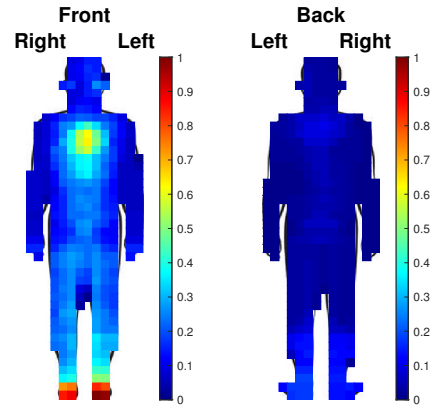


Figure 9: A combined result of all the on-body locations reported by the participants for the 14 modes used in this study. The graph highlights all the areas where sensations were perceived by participants.

Figure 6 were modes 9, 11, and 13, and their pressure fields could be divided into five segments, such that, each segment would contain either an area of high pressure or an area of low pressure. Therefore, a total of five segments were considered for each mode.

Segmenting Participant Data:

The participant data were normalized according to the maximum height of the participants. This was done to provide a fair comparison with the simulation results since height was likely to play a role in the on-body locations of sensations. The on-body location data provided in Fig. 12 were divided into five segments of equal height, i.e., the height of each segment was 183/5 cm. During

each trial, participants selected locations on a 2D silhouette representing on-body locations. These locations were allocated to the corresponding segments based on their height. In this way, each selected location from a trial was categorized into one of the five segments.

After collecting this data across all participants, we normalized the counts of selected locations to percentages, as shown in Fig. 10. The percentage value assigned to a given segment indicates the proportion of times that that segment was chosen out of all the body locations selected during the trial. This allows us to understand how often each segment was interacted with, in relation to the entire body, across different participants. This was repeated for all the modes.

Segmenting Simulation Data:

The same strategy was used to segment the simulation results for various modes. The simulated pressure field, a 3D grid, was first normalized, and the absolute pressure values were extracted. Two-dimensional pressure slices parallel to the participant orientation were extracted at the center of locations described in Fig. 6. The pressure field remained constant across the whole cuboid region, however, the slices were considered for comparison purposes only. These slices were the areas of pressure fields that were experienced by the users. The size of the 2D slices was 0.5×1.83 m, in accordance with the width of the cuboid region and the normalized height of the participants.

Each slice was divided into five segments. Each of these segments is analyzed to determine the pressure intensity that would occur in that specific area. The normalized pressure intensities are then populated into the pre-defined segments. The resulting percentages indicate the proportion of total pressure intensity that each segment contributes. Just as in the trial data from the experiment where participants select body locations, the percentage value for each segment in the simulation signifies the frequency with which that segment would be selected based on the simulated pressure intensities. This provides a way to compare the likelihood of different segments being chosen, which is shown in percentage values in Fig. 11.

7.2.2 Error Comparison. The percentages for the corresponding segments in each mode were compared using MAE. The results are provided in Table 3. An overall error of 10.66 % was recorded. This signifies that if a sensation was predicted by the simulation to occur at a particular location, it was not reported by participants 10.66 % times. The mode with the higher error was recorded for mode 14 at 20.89 %, while the segment with the lowest accuracy was segment one at 14.69 % accuracy. The discrepancies in this result are further explained in the following section.

7.3 Qualitative Matching with simulations

The body locations where participants felt sensations are provided in Fig. 12 revealing distinct patterns in sensation distribution across the 14 modes. Based on the simulation pressure distribution patterns in the cuboid regions of the experiment, the modes can be divided into three groups. Modes with uniform pressure in the vertical direction (1, 3, 5, 8, 12, and 14), modes with two high-pressure zones only at the top and bottom (2, 4, 6, 7, and 10), and modes with three pressure zones horizontally (9, 11, and 13).

Implicit analysis of Fig. 12 revealed that the simulated high-pressure areas within the cuboid largely dictated the location of sensations. The responses for uniform vertical modes spanned the whole body, those for the modes with two high-pressure zones produced sensation clusters on the feet and upper trunk area, while those for the three pressure zone modes indicated three rather distinct areas of sensation perception on the body.

While most modes closely follow their simulated pressure distributions, others (2, 4, 12) are influenced by additional factors such as participant orientation and emergent properties of frequency (discussed in Section 8.3), indicating that the sensation experience is not solely dictated by pressure fields. Detailed analysis of the modes is provided in Appendix B.

Most notably, the data shows that higher frequency modes have better focusing capabilities, allowing for more precise sensation localization. This could have significant implications for applications requiring high-resolution haptic feedback. Therefore, understanding these relationships between pressure fields and sensation locations could be pivotal for optimizing user experiences in future haptic systems.

An individual analysis of the participant response variability showed two distinct groups. One group consistently reported sensations across more body segments, while the other smaller group perceived them in fewer segments. This distinction was evident across different modes: when stimuli were expected to elicit sensations in all body segments, the first group typically reported four to five segments, whereas the second group, noted sensations in at most three segments. Similarly, in modes with less extensive stimuli, where the first group felt sensations in three to four segments, the second group usually reported feeling them in only one or two segments. This might be because some people only noted the strongest sensations and missed the weaker ones, they naturally paid more attention to specific segments, or their body composition made certain segments more sensitive.

It might appear that most modes produce similar sensory feedback at the same bodily locations; this is not a limitation but a feature. These modes have different spatial distributions within the room, allowing for a consistent sensory experience across various locations. This allows the use of different modes to achieve the same sensation in various areas of the room. However, it is important to acknowledge that this approach does have limitations in terms of the diversity and range of possible sensations. While it facilitates a uniform experience, it may restrict the variability and richness of sensory feedback that can be achieved.

8 RESULTS: VERBAL SENSATION DESCRIPTIONS

During the experiment, participants described the sensations they experienced as though relaying the information to someone else. Some participants offered elaborate descriptions, while others opted for single words or, in certain instances, gave no descriptions at all. Participants' verbal descriptors were categorized to identify recurring themes or to understand how the different modes are perceived by users. This categorization offered valuable insights into the overarching patterns in sensory perception. The descriptors were analyzed to search for the most commonly used terms,

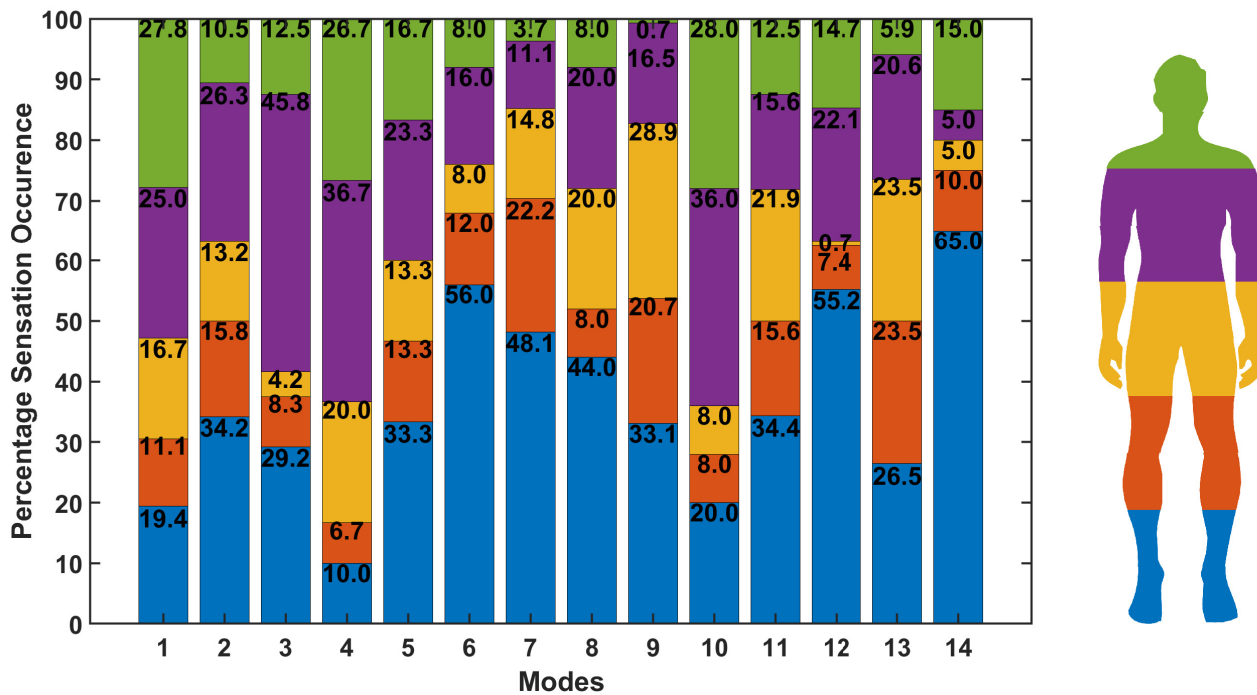


Figure 10: The percentages of sensation occurrence according to participants. The color of the bars indicates the different height segments as shown in the human silhouette on the right.

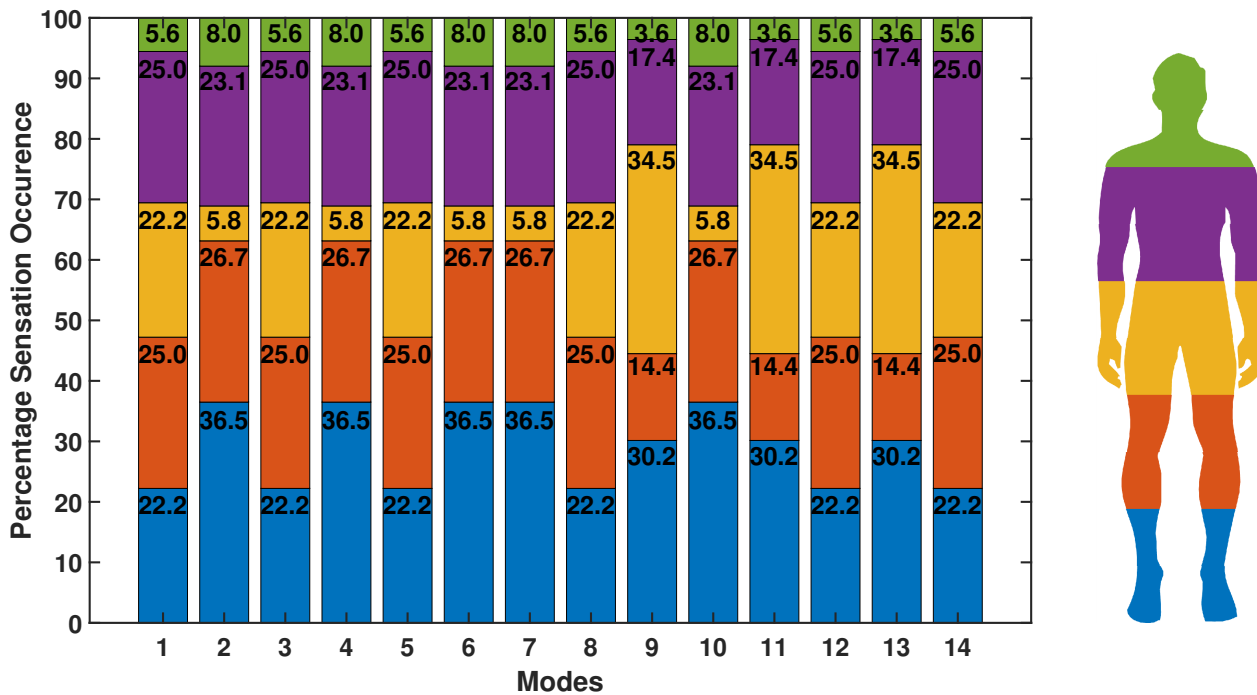


Figure 11: The percentages of sensation occurrence according to simulations at different heights of the body. The color of the bars indicates the different height segments as shown in the human silhouette on the right.

Modes	Segment 1	Segment 2	Segment 3	Segment 4	Segment 5	Mean Accuracy
	0.0 – 0.36	0.36 – 0.73	0.73 – 1.09	1.09 – 1.46	1.46 – 1.83	
1	2.78	13.89	5.56	0.00	22.22	8.89
2	2.28	10.87	7.39	3.21	2.55	5.26
3	6.94	16.67	18.06	20.83	6.94	13.89
4	26.49	19.99	14.23	13.56	18.69	18.59
5	11.11	11.67	8.89	1.67	11.11	8.89
6	19.51	14.66	2.23	7.11	0.02	8.71
7	11.66	4.43	9.05	12.00	4.27	8.28
8	21.78	17.00	2.22	5.00	2.44	9.69
9	2.94	6.33	5.58	0.85	2.83	3.70
10	16.49	18.65	2.23	12.89	20.03	14.06
11	4.22	1.27	12.66	1.77	8.93	5.77
12	32.96	17.64	21.56	2.92	9.16	16.85
13	3.68	9.18	11.00	3.20	2.31	5.87
14	42.78	15.00	17.22	20.00	9.44	20.89
Mean Accuracy	14.69	12.66	9.85	7.50	8.64	10.67

Table 3: The mean absolute error between the simulated and reported on-body location of sensations. The body is divided into five vertical segments, and error data for the 14 modes at each segment is provided.

check consistency with the simulated pressure fields, and search for emergent perceptual properties irrespective of the pressure fields.

8.1 Commonly used Descriptors

The most frequently occurring verbal descriptor used by the participants to describe the sensations was related to vibration. The term “vibration, vibrating, or vibrate” occurred 31 times, while the terms “shaking”, “tingling”, “tickle”, “tickling”, “buzzing”, and “pulsating” were also employed, used 5, 25, 9, 9, 5, and 5 times respectively. These can be considered as subtle variations of “vibration”, each reflecting different perceived intensities. For instance, the term “tingling or tickle” was mostly used when the participants perceived the feedback as mild or pleasant vibration. The term vibration was either linked with specific body parts, such as, “vibrating feet, or vibrating lower body” or used independently to describe the overall sensation, such as “vibrating or vibration”.

On the other hand, the term “pressure” was noted 42 times and “compressing” 6 times, typically in reference to internal sensations in the trunk region or the head. Participant responses include “Pressure inside the rib cage”, and “compressing pressure on organs”.

8.2 Sensation Consistency with Simulated Pressure

The objective of this analysis was to assess the degree to which the verbal descriptors provided by participants aligned with expectations based on simulated pressure profiles. This exercise not only serves to validate the computational models but also to illuminate any discrepancies that might have implications for the interpretation of sensory experiences. Some instances revealed a strong correlation between the simulated pressures and the participants’ verbal descriptions, while others did not, suggesting that perception of room modes is a complex phenomenon.

8.2.1 Consistent. Participants describing a sensation being perceived on their right or left side were consistent with the pressure

variations from simulations. Similarly, participants perceiving sensations on a specific portion of their body, such as lower body, feet, or head, were also in accordance with the simulations. Some examples from participant responses are provided for illustration: “numb hands, vibrating belly, dull head” (p6 for mode 1); “Vibration on whole feet but stronger on front of the feet, tingling effect on the soles of the feet” (p9 for mode 10); “vibration under both feet”, “From toe to hip vibrating”, “Slight vibration almost tickling feeling on feet and lower body” (p2, p7, and p13 for mode 7).

8.2.2 Contradictory. There were some instances where participants reported unexpected or opposite body locations than what was expected from simulations. For instance, a sensation that was supposed to be perceived on the right side of the body was reported to be stronger on the left side or vice versa. These mostly occurred when the pressure fields across the body were not consistent, such as in modes 4, 6, 7, and 10. From Fig. 6, it can be seen that the pressure fields in these modes diminish from side to side or front to back. Suppose a participant is positioned in Location 1 for Mode 7 (see Fig. 6g). Although the sensation is expected to be more intense on the participant’s left foot, a few participants reported experiencing the sensation on either both feet or exclusively on their right foot. Some participant responses, in this case, were; “Right leg”, “Both feet”, “vibration under both feet” by p8, p14, and p4, respectively. The role of the pressure field’s transition in the sensation being perceived on the opposite side appears likely, although its exact influence remains unclear.

8.3 Emergent Perceptual Properties

An implicit analysis of the qualitative descriptors pointed towards several emergent perceptual properties of the modes that manifested independently of the pressure fields. These perceptual properties were not predicted by the simulations or room locations, rather these seemed to be inherent to the modes that were played.

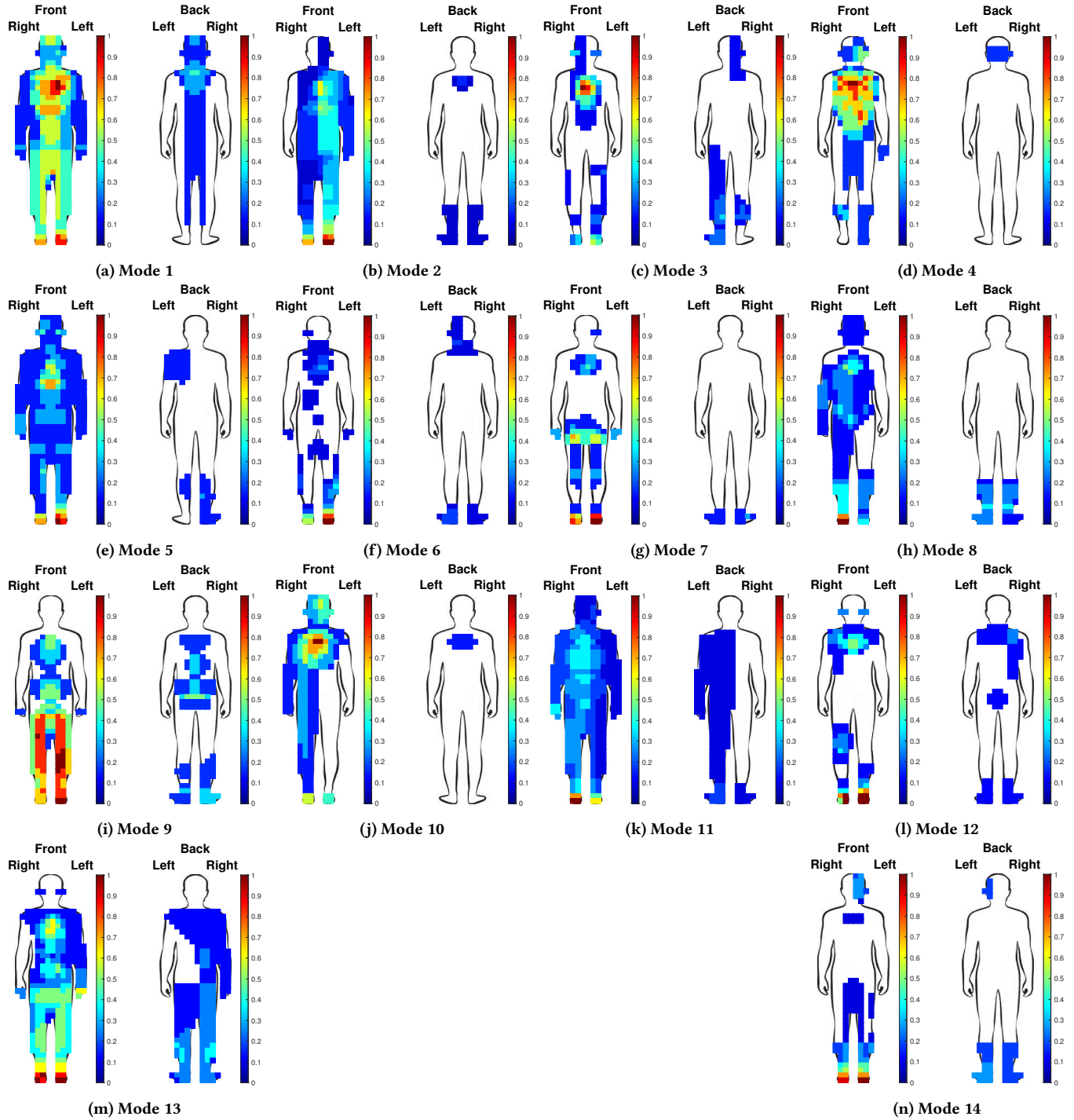


Figure 12: The sensation distribution on different parts of the body for the 14 modes, as reported by users in the experiment. Each subfigure displays two silhouettes, one for the front of the body and one for the backside. Data from the two physical locations in the experiment is combined for each mode.

It is interesting to note that such emergent properties existed and were unveiled during the study.

8.3.1 Within body sensations. A recurrent and consistent theme was that the lower frequency modes (modes 1 to 4) were associated

with sensations inside the body by most of the participants. One of the participant responses for mode 1 was “*I felt it from throat to feet but on the inside*”, another response for mode 1 was “*Pressure and vibrating of my organs*”. P13’s response for mode 2 was “*Vibrating, like the organs were moving inside the body, vibration filling almost whole body but arms are excluded*”. Similarly, p11 reported “*Seems whole body very slight vibration and some fullness*” for mode 4. Although the pressure fields for these modes differ in their distribution, the inside body sensations were felt consistently by most participants.

8.3.2 Focal point of the sensations within the body. Another emergent property reported by the participants was related to the size of the focal point or sensation radius for modes 1 to 4. They reported that the sensations within the body were widespread in the earlier modes and more focused as the frequencies got higher. Some responses for mode 4 were “*More focused than just before*” (p2), and “*Bit more focused and less spread than number 13*” (p13) (number 13 refers to the preceding trial which played mode 1). This trend continued till mode 6 for some participants. P10 commented for mode 6; “*Less widespread feeling than before but still wider than during the first 6 trials*”, the preceding trial played mode 3, and the first six trials had higher frequencies for this participant.

9 GENERAL DISCUSSION

The goal of this work was to introduce and evaluate non-contact whole-body sensations induced by low-frequency sounds. Before delving into how our technology uncovers new dimensions of haptic interaction, it is instructive to consider an analogy with ultrasound-based haptic technologies [6, 18]. Similar to the low-frequency sound-based haptics, ultrasound technologies initially faced skepticism and technical challenges [40]. However, years of research and refinement have enabled ultrasound-based haptics to offer precise and controllable user interactions.

In this context, our research marks an essential step in a similar trajectory for low-frequency sound-based haptics, aligning with Oulasvirta et al.’s [35] perspective on HCI as a field driven by problem-solving through evolving solutions. While the current focus of our study has been on understanding user perceptions in controlled scenarios, this is a foundational step towards more interactive applications. Acknowledging the limitations and initial focus on passive user experiences, our future research aims to explore and develop more dynamic interaction paradigms. This will involve studies that allow users to actively engage with and explore the haptic environment. The potential for adaptability and personalization in our approach aligns with the broader goals of HCI, as outlined in [35], emphasizing user-centric design and the exploration of innovative interaction modalities.

9.1 Non-contact Sensation On, In, and Across the Body

The questions raised about the feasibility of low-frequency sounds as a non-contact medium for delivery sensations have been answered by the results of the perceptual experiment. Here we discuss the different sensations that can be created using this system.

9.1.1 Inducing Non-contact Sensations. The results demonstrated that low-frequency sounds can successfully provide non-contact sensations on the body. This non-contact feedback can induce a range of sensations across different parts of the body. A noteworthy observation from the user responses was the frequent description of non-contact sensations as “vibration”. This phenomenon raises questions about the underlying mechanisms of sensory perception in this context. Could it be that the air pressure fluctuations induced by low-frequency sounds are sufficiently strong to cause vibrations in the clothing fabric or even the fine hairs on the skin surface? Alternatively, are we looking at a purely auditory phenomenon where high-energy low-frequency sounds are directly interpreted by humans as tactile vibrations? In a study by Landström et al., hearing and vibrotactile thresholds were measured for both normal-hearing and deaf subjects [24]. The results indicated that, in addition to hearing, another form of sensation related to vibration occurs at levels 20 to 25 dB above the hearing threshold. It shows that “feeling” the sound is separate from hearing it and that it carries sufficient energy to be felt by the body when played at a high enough amplitude. Similarly, these results were corroborated by another study which reported the threshold of body sensation to be 10 to 30 dB less sensitive [51]. They recorded on-body sensations while subjecting the whole body to low-frequency sounds, and then the body without the head. It was reported that the sensations were perceived in both conditions but the threshold of perception was higher for the second condition.

These studies suggest the feasibility of using low-frequency sounds for delivering non-contact sensations, however, they do not report the mechanism through which it appears to happen. It would be interesting to find out if the sounds directly vibrate the body, vibrate the clothes or hair on the body which in turn are felt as sensations on the body. An experiment could be designed that exposes covered and exposed parts of the body and finds out where the sensations are recorded.

9.1.2 Within-body Sensation: A New Frontier. The low frequency sounds were also felt inside the body by almost all the participants, highlighting our system’s capability to deliver non-contact within-body sensations. This is a feature unique to low-frequency sound-based haptics and is hard to achieve with other haptic technologies. For example, the lower frequency modes were recurrently described as producing sensations that participants felt originated “inside” their bodies, often akin to internal vibration. On one hand, the within-body sensations were felt as “vibrating organs” or “pressure on the chest”. On the other hand, they were perceived as a “nice feeling” or a “warm, diffused sensation throughout the body”. In contrast, the experiences induced by higher frequency modes were more superficial, described as being on the skin or at the body surface, such as, “tingling” or “something moving on my skin”.

This effect can be likened to the effect of infrasound (frequencies below 20 Hz). Infrasound has been reported to cause feelings of awe or fear, chills, and other unusual sensations [28, 47], and in some cases physiological effects [37, 52]. Our system was able to induce sensations robustly across all the participants, however, in the current study we did not rate the emotional state of the users.

It can be an interesting avenue to explore the emotional aspects of non-contact low frequency sounds.

9.1.3 Local and Global Sensations. The data suggest that modes target bodily sensations differently. Higher frequency modes had better focusing capabilities, allowing for sensations to be localized more precisely on the body. For example, modes 9 and 13 exhibited well-defined sensation zones on the body. The focus on specific body parts like the feet and upper trunk in modes 6, 7, and 10 further emphasizes the system's capability for localized sensations. On the other hand, modes 1, 5, and 8 led to sensations that were dispersed across various body regions, suggesting a more global sensory experience. Thus, low-frequency sounds can be used to induce non-contact localized and global sensations offering a multi-modal approach to haptic feedback. Different modes could be deployed together to achieve a blend of localized and global sensations.

Only a handful of haptic systems can provide local and global feedback, such as haptic suits or vests [20, 46]. These systems can focus on larger areas of the body or specific parts at a time. In comparison to our system, they can provide more precise and controllable feedback. However, the non-contact capability of our system makes it a promising alternative.

9.2 How to Create Sensations Reliably

We found a mismatch of only 10.66 % between simulated and recorded high-pressure areas. Along with the sensations described by participants, suggesting that low-frequency sounds could be directed to elicit specific sensory outcomes. The consistency in descriptors used by participants suggests that the induced sensations were achieved reliably. The perceptual characterization study revealed that not only could basic sensations be induced, but more complex sensory experiences could also be reliably generated across a significant number of participants. This consistency was corroborated by the on-body sensation location data, which demonstrated similar areas of sensory perception among different individuals.

A collective view of the verbal descriptors and the on-body locations can provide a method of creating body-location-specific or perception-specific sensations. The location data dictates the regions of the body “where” sensations will be perceived, whereas, the verbal descriptions tell us “how” the user will perceive it. In addition to these, the simulated pressure fields can provide the areas in the room where sensations are likely to be stronger. A combination of these data can be used by an algorithm to generate specific sensations in user’s body at different locations in the room. For instance, participants described mode 1 as being the most diffused sensation around the trunk area; according to the emergent properties, mode 1 manifested inside the body for most participants; and according to the on-body location information, mode 1 mostly manifested in the upper region of the chest. Using the collective findings of all these results, a diffused feeling of pressure around the upper chest area can be successfully achieved using mode 1.

The height segments provided in Section 7 can be considered as the minimum surface area that can be targeted using the current system. It was empirically noted that smaller regions can also be targeted, however, these were not experimentally validated in the current study. Another interesting aspect was the detectability of edges between areas of high and low pressure. Although not

experimentally corroborated, the edges were distinctly perceivable when moving around in the room.

9.3 Use Case Scenarios

The following use cases highlight how non-contact low-frequency sounds can be used in different applications. These use cases permit the walk-up-and-play paradigm without forcing the user to wear or touch any device. The users enter the interaction space and become a part of a multi-sensory experience, receiving tactile feedback that seamlessly integrates with the visual and auditory elements.

Using this technology users can enter an art exhibition with pictures of boats hanging on the walls. A speaker will be playing the audible sound of breeze and seagulls. Low-frequency sound is emitted with varying frequencies so that their resonant modes contain high amplitude at positions that slowly swing along the user’s body, simulating the waves undulating smoothly on the seashore. Turning the sensations on and off can produce a feeling of waves touching the body.

Another scenario is an immersive cave with projected images or big screens on the walls. As in a traditional cave, the user gets 360° visual information. Non-contact sensations can be induced using low-frequency sounds that match the visual content. A common problem of 360° content is to indicate to the user that they should be looking at a specific position [48]. Haptic feedback, in addition to increased immersion, can also be used to direct the user’s attention.

Therapeutic massage sessions can involve people sitting or lying down with their eyes closed as they usually would in a traditional massage parlor. However, instead of hands-on treatment, they receive low-frequency sounds that induce sensations either on or within the body, depending on client preference and therapeutic needs. Its non-contact nature makes it a hygienic alternative to traditional massage, suitable for a variety of clients including those who may be touch-averse or have specific medical conditions. Especially, elderly individuals who may find traditional massage techniques too aggressive.

Volumetric fog screens [23] would benefit from being able to provide haptic feedback to the users who introduce their hands into the display volume. The display would induce local sensations on their hands. Even if the spatial resolution of the resonant modes does not allow for fine control of the feedback position, events such as clicking, canceling, or going back could have associated coarse sensations in the user’s hand that is inside the display.

A significant number of VR and gaming environments already take place in enclosed spaces. Enriching the user experience by adding non-contact low-frequency sounds could open up new possibilities for interaction design, virtual reality, gaming, and many other applications. With careful design and implementation, it is possible to create a non-contact haptic workspace that provides a unique and immersive user experience [40, 45].

9.4 Limitations

The use of low-frequency sounds for haptic feedback presents a novel approach to immersive experiences, yet, it comes with its own set of challenges. One of the primary concerns is the potential health implications. Prolonged exposure to infrasound or low-frequency sounds, at very high amplitudes, has been associated

with symptoms such as fatigue, sleep disturbances, and a sensation of pressure in the ears [39]. However, in our current system, the sound levels are well within the safety limits (max 113 dB), and with hearing protection, the users do not feel annoyance or discomfort. The U.S. Occupational Safety and Health Administration (OSHA) specifies that noise exposure should never exceed 140 dB in any circumstance without hearing protection [42].

The sound levels required for effective sensation can be between 90 dB and 110 dB, which could be disruptive or uncomfortable for the user and those in the surrounding environment. The system might also require confined spaces to effectively control and direct the sound waves, limiting its applicability in open or large areas. However, the size of the room is not a significant factor and the simulations can be run for different sizes. Furthermore, significant changes in the environment, such as the introduction of large objects or alterations in the physical layout of the room, could necessitate recalibration of the system to maintain effective haptic feedback. Depending on the modes in use, the sealing criterion changes. A room is considered acoustically sealed if the cracks or crevices are smaller than the wavelength of the frequencies used.

The sample size, though sufficient for initial exploration, may need to be expanded to generalize the findings. In addition, more control parameters can be introduced to see their effect on the induced sensations. For instance, the orientation of the user, towards or away from the source, might have a significant effect on the body location or intensity of sensations. Similarly, different amplitudes for different modal frequencies could also provide insights into how the intensity of sensations is perceived by users.

10 CONCLUSION

We proposed and evaluated a non-contact haptic feedback system based on low-frequency sounds. We were able to induce sensations within the body, on the whole body, and on parts of the body. The location of these sensations was largely dictated by the pressure fields that were generated by simulating the modal response of a confined room. The validity of the simulation was first confirmed with pressure recordings in the real room. Later these simulations were used to guide the experimental design. The results of the perceptual study validated the simulated pressure field predictions and proved that low-frequency sounds can be used to induce bodily sensations reliably.

ACKNOWLEDGMENTS

This work is funded by the European Union's Horizon 2020 research and innovation programme [grant number 101017746, TOUCHLESS].

REFERENCES

- [1] Muhammad Abdullah, Minji Kim, Waseem Hassan, Yoshihiro Kuroda, and Seokhee Jeon. 2018. HapticDrone: An encountered-type kinesthetic haptic interface with controllable force feedback: Example of stiffness and weight rendering. In *2018 IEEE Haptics Symposium (HAPTICS)*. IEEE, San Francisco, CA, USA, 334–339. <https://doi.org/10.1109/HAPTICS.2018.8357197>
- [2] Adilzhan Adilkhanov, Matteo Rubagotti, and Zhanat Kappassov. 2022. Haptic devices: Wearability-based taxonomy and literature review. *IEEE Access* 10 (2022), 91923–91947. <https://doi.org/10.1109/ACCESS.2022.3202986>
- [3] Mudassir Ibrahim Awan, Ahsan Raza, and Seokhee Jeon. 2023. DroneHaptics: Encountered-Type Haptic Interface Using Dome-Shaped Drone for 3-DoF Force Feedback. In *2023 20th International Conference on Ubiquitous Robots (UR)*. IEEE, Honolulu, HI, USA, 195–200. <https://doi.org/10.1109/UR57808.2023.10202318>
- [4] Mahdi Azmandian, Mark Hancock, Hrvoje Benko, Eyal Ofek, and Andrew D Wilson. 2016. Haptic retargeting: Dynamic repurposing of passive haptics for enhanced virtual reality experiences. In *Proceedings of the 2016 CHI Conference on Human Factors in Computing Systems* (San Jose, California, USA). Association for Computing Machinery, New York, NY, USA, 1968–1979. <https://doi.org/10.1145/2858036.2858226>
- [5] Sophia Brueckner and Rachel Freire. 2018. Embodisuit: a wearable platform for embodied knowledge. In *Proceedings of the Twelfth International Conference on Tangible, Embedded, and Embodied Interaction*. Association for Computing Machinery, New York, NY, USA, 542–548. <https://doi.org/10.1145/3173225.3173305>
- [6] Tom Carter, Sue Ann Seah, Benjamin Long, Bruce Drinkwater, and Sriram Subramanian. 2013. UltraHaptics: multi-point mid-air haptic feedback for touch surfaces. In *Proceedings of the 26th annual ACM symposium on User interface software and technology*. Association for Computing Machinery, New York, NY, USA, 505–514. <https://doi.org/10.1145/2501988.2502018>
- [7] Lung-Pan Cheng, Eyal Ofek, Christian Holz, Hrvoje Benko, and Andrew D Wilson. 2017. Sparse haptic proxy: Touch feedback in virtual environments using a general passive prop. In *Proceedings of the 2017 CHI Conference on Human Factors in Computing Systems* (Denver, Colorado, USA). Association for Computing Machinery, New York, NY, USA, 3718–3728. <https://doi.org/10.1145/3025453.3025753>
- [8] Heather Culbertson, Samuel B Schorr, and Allison M Okamura. 2018. Haptics: The present and future of artificial touch sensation. *Annual Review of Control, Robotics, and Autonomous Systems* 1 (2018), 385–409. <https://doi.org/10.1146/annurev-control-060117-105043>
- [9] Wang Dangxiao, Guo Yuan, Liu Shiyi, Yuru Zhang, Xu Weiliang, and Xiao Jing. 2019. Haptic display for virtual reality: progress and challenges. *Virtual Reality & Intelligent Hardware* 1, 2 (2019), 136–162. <https://doi.org/10.3724/SP.J.2096-5796.2019.0008>
- [10] Julia C Duvall, Lucy E Dunne, Nicholas Schleif, and Brad Holschuh. 2016. Active "hugging" vest for deep touch pressure therapy. In *Proceedings of the 2016 ACM international joint conference on pervasive and ubiquitous computing: adjunct*. Association for Computing Machinery, New York, NY, USA, 458–463. <https://doi.org/10.1145/2968219.2971344>
- [11] Emma Frid and Hans Lindetorp. 2020. Haptic Music: Exploring Whole-Body Vibrations and Tactile Sound for a Multisensory Music Installation. In *Sound and Music Computing Conference Torino, June 24th-26th 2020*. CERN, Torino, Italy, 68–75.
- [12] Emma Frid, Hans Lindetorp, Kjetil Falkenberg Hansen, Ludvig Elblaus, and Roberto Bresin. 2019. Sound forest: evaluation of an accessible multisensory music installation. In *Proceedings of the 2019 CHI Conference on Human Factors in Computing Systems*. Association for Computing Machinery, New York, NY, USA, 1–12. <https://doi.org/10.1145/3290605.3300907>
- [13] Shogo Fukushima and Hiroyuki Kajimoto. 2012. Facilitating a surprised feeling by artificial control of piloerection on the forearm. In *Proceedings of the 3rd Augmented Human International Conference*. Association for Computing Machinery, New York, NY, USA, 1–4. <https://doi.org/10.1145/2160125.2160133>
- [14] James Gay, Moritz Umfahrer, Arthur Theil, Lea Buchweitz, Eva Lindell, Li Guo, Nils-Krister Persson, and Oliver Korn. 2020. Keep your distance: a playful haptic navigation wearable for individuals with deafblindness. In *Proceedings of the 22nd International ACM SIGACCESS Conference on Computers and Accessibility*. Association for Computing Machinery, New York, NY, USA, 1–4. <https://doi.org/10.1145/3373625.3418048>
- [15] Sidhant Gupta, Dan Morris, Shwetak N Patel, and Desney Tan. 2013. Airwave: Non-contact haptic feedback using air vortex rings. In *Proceedings of the 2013 ACM international joint conference on Pervasive and ubiquitous computing*. Association for Computing Machinery, New York, NY, USA, 419–428. <https://doi.org/10.1145/2493432.2493463>
- [16] Vincent Hayward, Oliver R Astley, Manuel Cruz-Hernandez, Danny Grant, and Gabriel Robles-De-La-Torre. 2004. Haptic interfaces and devices. *Sensor review* 24, 1 (2004), 16–29. <https://doi.org/10.1108/02602280410515770>
- [17] Naros Iriarte, Iñigo Ezcurdia, Sonia Elizondo, José Irisarri, Daria Hemmerling, Amalia Ortiz, and Asier Marzo. 2023. Contactless Electrostatic Piloerection for Haptic Sensations. *IEEE Transactions on Haptics* (2023), 1–12. <https://doi.org/10.1109/TOH.2023.3269885>
- [18] Takayuki Iwamoto, Mari Tatezono, and Hiroyuki Shinoda. 2008. Non-contact method for producing tactile sensation using airborne ultrasound. In *Haptics: Perception, Devices and Scenarios: 6th International Conference, EuroHaptics 2008 Madrid, Spain, June 10–13, 2008 Proceedings 6*. Springer, Berlin, Heidelberg, 504–513. https://doi.org/10.1007/978-3-540-69057-3_64
- [19] Lynette A Jones. 2016. Perspectives on the evolution of tactile, haptic, and thermal displays. *MIT Open Access Articles* 25, 3 (2016), 247–252. https://doi.org/10.1162/PRES_a_00266
- [20] Daeseok Kang, Chang-Gyu Lee, and Ohung Kwon. 2023. Pneumatic and acoustic suit: multimodal haptic suit for enhanced virtual reality simulation. *Virtual Reality* 27, 3 (2023), 1–23. <https://doi.org/10.1007/s10055-023-00756-5>

- [21] Yusuke Kishishita, Swagata Das, Antonio Vega Ramirez, Chetan Thakur, Ramin Tadayon, and Yuichi Kurita. 2019. Muscleblazer: Force-feedback suit for immersive experience. In *2019 IEEE Conference on Virtual Reality and 3D User Interfaces (VR)*. IEEE, Osaka, Japan, 1813–1818. <https://doi.org/10.1109/VR2019.8797962>
- [22] Yukari Konishi, Nobuhisa Hanamitsu, Benjamin Outram, Kouta Minamizawa, Tetsuya Mizuguchi, and Ayahiko Sato. 2016. Synesthesia suit: the full body immersive experience. In *ACM SIGGRAPH 2016 VR Village*. Association for Computing Machinery, New York, NY, USA, 1–1. <https://doi.org/10.1145/2929490.2932629>
- [23] Miu-Ling Lam, Yaozhun Huang, and Bin Chen. 2015. Interactive volumetric fog display. In *SIGGRAPH Asia 2015 Emerging Technologies*. Association for Computing Machinery, New York, NY, USA, 1–2. <https://doi.org/10.1145/2818468.2818488>
- [24] Ulf Landström, Ronnie Lundström, and Marianne Byström. 1983. Exposure to infrasound—perception and changes in wakefulness. *Journal of Low Frequency Noise, Vibration and Active Control* 2, 1 (1983), 1–11. <https://doi.org/10.1177/02630923800200101>
- [25] Stephen D Laycock and AM Day. 2003. Recent developments and applications of haptic devices. In *Computer Graphics Forum*, Vol. 22. Wiley Online Library, Blackwell Publishing, Inc., Oxford, UK, 117–132. <https://doi.org/10.1111/1467-8659.00654>
- [26] Stephen D Laycock and AM Day. 2007. A survey of haptic rendering techniques. In *Computer graphics forum*, Vol. 26. Wiley Online Library, Blackwell Publishing, Inc., Oxford, UK, 50–65. <https://doi.org/10.1111/j.1467-8659.2007.00945.x>
- [27] Myungho Lee, Gerd Bruder, and Gregory F Welch. 2017. Exploring the effect of vibrotactile feedback through the floor on social presence in an immersive virtual environment. In *2017 IEEE Virtual Reality (VR)*. IEEE, Los Angeles, CA, USA, 105–111. <https://doi.org/10.1109/VR.2017.7892237>
- [28] Henry Scott Macdonald, Betty Yin, Danyon Wye, Bridget Hall, and Paul Ralph. 2017. Increasing the Emotionality of Horror Games with Infrasound. In *Proceedings of the DiGRA 2017 Conference: Think Design Play*. DiGRA, Melbourne, Australia, 2–6. <https://api.semanticscholar.org/CorpusID:173985933>
- [29] Maurizio Maisto, Claudio Pacchierotti, Francesco Chinello, Gionata Salvietti, Alessandro De Luca, and Domenico Prattichizzo. 2017. Evaluation of wearable haptic systems for the fingers in augmented reality applications. *IEEE transactions on haptics* 10, 4 (2017), 511–522. <https://doi.org/10.1109/TOH.2017.2691328>
- [30] Yasutoshi Makino, Yoshikazu Furuyama, Seki Inoue, and Hiroyuki Shinoda. 2016. Haptoclone (Haptic-Optical Clone) for Mutual Tele-Environment by Real-time 3D Image Transfer with Midair Force Feedback. In *Proceedings of the 2016 CHI Conference on Human Factors in Computing Systems*, Vol. 16. Association for Computing Machinery, New York, NY, USA, 1980–1990. <https://doi.org/10.1145/2858036.2858481>
- [31] Victor Rodrigo Mercado, Maud Marchal, and Anatole Lécuyer. 2021. “Haptics on-demand”: A survey on encountered-type haptic displays. *IEEE Transactions on Haptics* 14, 3 (2021), 449–464. <https://doi.org/10.1109/TOH.2021.3061150>
- [32] Henrik Møller and Christian Sejer Pedersen. 2004. Hearing at low and infrasonic frequencies. *Noise & health* 6, 23 (2004), 37–57.
- [33] Taha Moriyama and Hiroyuki Kajimoto. 2021. HARVEST: High-resolution haptic vest and fingertip sensing glove that transfers tactile sensation of fingers to the back. *Applied Sciences* 11, 3 (2021), 1298. <https://doi.org/10.3390/app11031298>
- [34] Soroosh Mortezapoor, Khrystyna Vasylevska, Emanuel Vonach, and Hannes Kaufmann. 2023. CoboDeck: A Large-Scale Haptic VR System Using a Collaborative Mobile Robot. In *2023 IEEE Conference Virtual Reality and 3D User Interfaces (VR)*. IEEE, Shanghai, China, 297–307. <https://doi.org/10.1109/VR55154.2023.000045>
- [35] Antti Oulasvirta and Kasper Hornbaek. 2016. HCI research as problem-solving. In *Proceedings of the 2016 CHI Conference on Human Factors in Computing Systems* (San Jose, California, USA). Association for Computing Machinery, New York, NY, USA, 4956–4967. <https://doi.org/10.1145/2858036.2858283>
- [36] Claudio Pacchierotti, Stephen Sinclair, Massimiliano Solazzi, Antonio Frisoli, Vincent Hayward, and Domenico Prattichizzo. 2017. Wearable haptic systems for the fingertip and the hand: taxonomy, review, and perspectives. *IEEE transactions on haptics* 10, 4 (2017), 580–600. <https://doi.org/10.1109/TOH.2017.2689006>
- [37] Michael A Persinger. 2014. Infrasound, human health, and adaptation: an integrative overview of recondite hazards in a complex environment. *Natural Hazards* 70, 1 (2014), 501–525. <https://doi.org/10.1007/s11069-013-0827-3>
- [38] Helena Pongrac. 2008. Vibrotactile perception: examining the coding of vibrations and the just noticeable difference under various conditions. *Multimedia systems* 13, 4 (2008), 297–307. <https://doi.org/10.1007/s00530-007-0105-x>
- [39] Ville Rajala, Jarkko Hakala, Reijo Alakoivu, Ville Koskela, and Valtteri Hongisto. 2022. Hearing threshold, loudness, and annoyance of infrasonic versus non-infrasonic frequencies. *Applied Acoustics* 198 (2022), 108981. <https://doi.org/10.1016/j.apacoust.2022.108981>
- [40] Ismo Rakkolainen, Euan Freeman, Antti Sand, Roope Raisamo, and Stephen Brewster. 2020. A survey of mid-air ultrasound haptics and its applications. *IEEE Transactions on Haptics* 14, 1 (2020), 2–19. <https://doi.org/10.1109/TOH.2020.3018754>
- [41] Alma G Rodríguez Ramírez, Francesco J García Luna, Osslan Osiris Vergara Villegas, and Manuel Nandayapa. 2018. *Applications of Haptic Systems in Virtual Environments: A Brief Review*. Springer, Cham. 349–377 pages. https://doi.org/10.1007/978-3-319-77770-2_13
- [42] Occupational Safety and Health Administration. 2008. *29 CFR 1910.95*. National Archives, Washington D.C. <https://www.osha.gov/laws-regulations/standardnumber/1910/1910.95> Accessed: 14 September 2024.
- [43] Rajinder Sodhi, Ivan Poupyrev, Matthew Glisson, and Ali Israr. 2013. AIREAL: interactive tactile experiences in free air. *ACM Transactions on Graphics (TOG)* 32, 4 (2013), 1–10. <https://doi.org/10.1145/2461912.2462007>
- [44] Daniel Spelmezan, Deepak Ranjan Sahoo, and Sriram Subramanian. 2017. Sparkle: Hover feedback with touchable electric arcs. In *Proceedings of the 2017 CHI Conference on Human Factors in Computing Systems*. Association for Computing Machinery, New York, NY, USA, 3705–3717. <https://doi.org/10.1145/3024543.3025782>
- [45] Vic Tandy and Tony R Lawrence. 1998. The ghost in the machine. *Journal-Society for Psychical Research* 62 (1998), 360–364. <https://doi.org/10.1592/phco.29.4.363>
- [46] TeslaSuit. 2016. TeslaSuit – Full Body Haptic VR Suit. <https://teslasuit.io/>. Accessed on 2023-07-18.
- [47] Raquel Thiessen, Daniel J Rea, Diljot S Garcha, Cheng Cheng, and James E Young. 2019. Infrasound for HRI: a robot using low-frequency vibrations to impact how people perceive its actions. In *2019 14th ACM/IEEE International Conference on Human-Robot Interaction (HRI)*. IEEE, Daegu, South Korea, 11–18. <https://doi.org/10.1109/HRI.2019.8673172>
- [48] Jan Oliver Wallgrün, Mahda M Bagher, Pejman Sajjadi, and Alexander Klippel. 2020. A comparison of visual attention guiding approaches for 360 image-based vr tours. In *2020 IEEE Conference on Virtual Reality and 3D User Interfaces (VR)*. IEEE, Atlanta, GA, USA, 83–91. <https://doi.org/10.1109/VR46266.2020.00026>
- [49] Dangxiao Wang, Meng Song, Afzal Naqash, Yukai Zheng, Weiliang Xu, and Yuru Zhang. 2018. Toward whole-hand kinesthetic feedback: A survey of force feedback gloves. *IEEE transactions on haptics* 12, 2 (2018), 189–204. <https://doi.org/10.1109/TOH.2018.2879812>
- [50] Pingjun Xia. 2018. New advances for haptic rendering: state of the art. *The Visual Computer* 34 (2018), 271–287. <https://doi.org/10.1007/s00371-016-1324-y>
- [51] S Yamada, M Ikuji, S Fujikata, T Watanabe, and T Kosaka. 1983. Body sensation of low frequency noise of ordinary persons and profoundly deaf persons. *Journal of Low Frequency Noise, Vibration and Active Control* 2, 3 (1983), 32–36. <https://doi.org/10.1177/02630923800200302>
- [52] Stanislav Ziaran et al. 2014. The assessment and evaluation of low-frequency noise near the region of infrasound. *Noise and health* 16, 68 (2014), 10. <https://doi.org/10.4103/1463-1741.127848>

A MAE OF SIMULATED PRESSURE AND RECORDED SIGNALS

The color of each point in Fig. 13 shows the magnitude of recorded values at that location in the room, while the size of the point represents the error between the predicted and recorded values. A comparison of Fig. 13 with Fig. 2 demonstrates a strong agreement between simulated and recorded fields in the high-pressure regions. In contrast, areas of low pressure exhibited substantial errors when evaluated through the Mean Absolute Error (MAE). The larger errors between areas of low pressure also played a significant role in the MAE being relatively high overall. Given that the focus of this study is on regions of high pressure for haptic sensations, the discrepancies in low-pressure areas are less consequential.

B QUALITATIVE MATCHING WITH SIMULATIONS

This section discusses the body locations reported by participants in the presence of different modes. As mentioned in Sect. 7.3, the modes were divided into three groups based on simulation pressure distributions.

It must be noted that the overall pressure distributions of modes within these groups might be significantly different, and this classification only takes into account the cuboid regions where the experiment was conducted. Each of these groups will be analyzed individually, as sensations elicited within these clusters are anticipated to exhibit similar patterns.

Mode		z_1					z_2					z_3				
		y_1	y_2	y_3	y_4	y_5	y_1	y_2	y_3	y_4	y_5	y_1	y_2	y_3	y_4	y_5
1	x_1	0.09	0.18	0.79	0.39	0.18	0.18	0.10	0.77	0.29	0.67	0.17	0.09	0.63	0.34	0.12
	x_2	0.22	0.01	0.55	0.16	0.30	0.68	0.76	0.22	0.03	0.24	0.11	0.18	0.74	0.41	0.06
	x_3	0.31	0.10	0.39	0.05	0.55	0.21	0.07	0.62	0.37	0	0.07	0.20	0.74	0.44	0.02
2	x_1	0.07	0.03	0	0.02	0.13	0.18	0.13	0	0.15	0.61	0.16	0.18	0.16	0.10	0.10
	x_2	0.19	0.18	0.19	0.24	0.24	0.84	0.30	1.00	0.64	0.50	0.11	0.10	0	0.04	0.06
	x_3	0.31	0.29	0.41	0.43	0.51	0.34	0.22	0.35	0.18	0.09	0.09	0.05	0.06	0	0.01
3	x_1	0.32	0.18	0.04	0.16	0.43	0.31	0.15	0.11	0.10	0.26	0.18	0.06	0.08	0	0.04
	x_2	0.23	0.28	0.27	0.43	0.49	0.08	0.27	0.20	0.08	0.08	0.11	0	0.21	0.03	0.25
	x_3	0.05	0.02	0.05	0	0.01	0.07	0.05	0.05	0	0	0.44	0.37	0.45	0.41	0.55
4	x_1	0	0.15	0.65	0.15	0.05	0.01	0.23	0.71	0.41	0	0.13	0.16	0.73	0.42	0.02
	x_2	0.22	0.12	0.10	0.48	0.60	0.79	0.48	0.22	0.33	0.89	0.95	0.31	0.14	0.30	0.55
	x_3	0.48	0.19	0.44	0.21	0.17	0.16	0.10	0.66	0.34	0.09	0.01	0.23	0.76	0.42	0.04
5	x_1	0.29	0.01	0.78	0.30	0.55	0.01	0.21	0.39	0.21	0	0.08	0.22	0.69	0.40	0.04
	x_2	0.34	0.29	0.26	0.32	0.39	0.35	0.36	0.18	0.29	0.43	0.26	0.21	0.28	0.35	0.13
	x_3	0.13	0.06	0.56	0.28	0.20	0.22	0.02	0.46	0.06	0.55	0.08	0.23	0.76	0.43	0
6	x_1	0.24	0.17	0	0.09	0.40	0	0.07	0.42	0.31	0.11	0.04	0.01	0.06	0.03	0.06
	x_2	0.35	0.24	0.13	0.22	0.44	0.33	0.32	0.02	0.18	0.39	0.32	0.27	0.15	0.25	0.07
	x_3	0.13	0.13	0.19	0.10	0.11	0.19	0.28	0.30	0.45	0.62	0.04	0	0.02	0	0.02
7	x_1	0.01	0.05	0.76	0.03	0	0.03	0.07	0.14	0.06	0	0.31	0.13	0.78	0.39	0.33
	x_2	0.51	0.24	0.57	0.19	0.50	0.51	0.44	0.33	0.17	0.53	0.02	0.09	0.70	0.35	0.18
	x_3	0.29	0.07	0.69	0.33	0.20	0.69	0.35	0.55	0.09	1.00	0.07	0.01	0.28	0.07	0.17
8	x_1	0	0.16	0.02	0.01	0.04	0.04	0.38	0.38	0.09	0.04	0.31	0.08	0	0.40	0.48
	x_2	0.08	0.17	0.18	0	0.12	0.03	0.25	0.36	0.20	0.06	0.22	0.16	0.10	0.10	0.22
	x_3	0.45	0.25	0.07	0.37	0.53	0.24	0.43	0.20	0.07	0.26	0.11	0.02	0.29	0.32	0.03
9	x_1	0.06	0.73	0.14	0.26	0	0.02	0.07	0.02	0.15	0	0.01	0.45	0.01	0.12	0.03
	x_2	0.06	0.82	0.04	0.15	0.01	0.01	0.07	0.01	0.15	0.01	0.02	0.45	0	0.33	0
	x_3	0.02	0.22	0.02	0.03	0.01	0.01	0.22	0.02	0.41	0.01	0.02	1.00	0	0.31	0.04
10	x_1	0.02	0.15	0.01	0.17	0.04	0.42	0.09	0.49	0.11	0.42	0.07	0.09	0.20	0.01	0.10
	x_2	0.07	0.27	0.44	0.07	0.05	0.39	0.11	0.62	0.51	0.34	0.03	0.13	0.06	0.18	0.06
	x_3	0.47	0.15	0.44	0.21	0.37	0.01	0.38	0.87	0.16	0.04	0	0.03	0	0.31	0.05
11	x_1	0.03	0.33	0.76	0.27	0	0.29	0.25	0.34	0.16	0.26	0.03	0.28	0.71	0.10	0.04
	x_2	0.04	0.08	0.69	0.01	0.01	0.46	0.77	0.29	0.27	0.65	0.01	0.07	0.76	0.17	0.03
	x_3	0.13	0.75	0.69	0.02	0.09	0.03	0.02	0.09	0.02	0	0.01	0.30	0.78	0.30	0.02
12	x_1	0.16	0.44	0.02	0.29	0.24	0.09	0.18	0.28	0.23	0.05	0	0.33	0	0.38	0.02
	x_2	0.63	0.58	0.71	0.78	0.63	0.47	0.22	0.46	0.46	0.37	0.68	0.53	0.65	0.41	0.65
	x_3	0.03	0.24	0.01	0.38	0.04	0.05	0.48	0.20	0.12	0.04	0.13	0.06	0.20	0.01	0.18
13	x_1	0.04	0.70	0.01	0.03	0.01	0.02	0.15	0.04	0.24	0.02	0.03	0.68	0	0.04	0.04
	x_2	0.36	0.34	0.67	0.61	0.33	0.29	0.23	0.36	0.13	0.26	0.50	0.02	0.51	0.27	0.51
	x_3	0.02	0.37	0.03	0.03	0	0	0.04	0.04	0.71	0	0.09	0.74	0.04	0.15	0.13
14	x_1	0.69	0.87	0.10	0.53	0.81	0.12	0.07	0.82	0.16	0.13	0.07	0.40	0.05	0.48	0.09
	x_2	0.63	0.22	0.06	0.11	0.51	0.66	0.47	0.30	0.33	0.57	0.80	0.51	0.57	0.58	0.65
	x_3	0.11	0.09	0.08	0.07	0.13	0.13	0.45	0.28	0.63	0.15	0.08	0.54	0.13	0.07	0.02

Table 4: The normalized error between the simulated and recorded pressure values at 45 different locations in the room. The locations are $x = \{0.1, 0.9, 1.6\}$, $y = \{0.1, 0.5, 1.0, 1.5, 2.1\}$, $z = \{0.3, 1.0, 1.7\}$. The boldface values represent the error when simulation pressure values exceed 80 % of the maximum, while the red values represent the remaining.

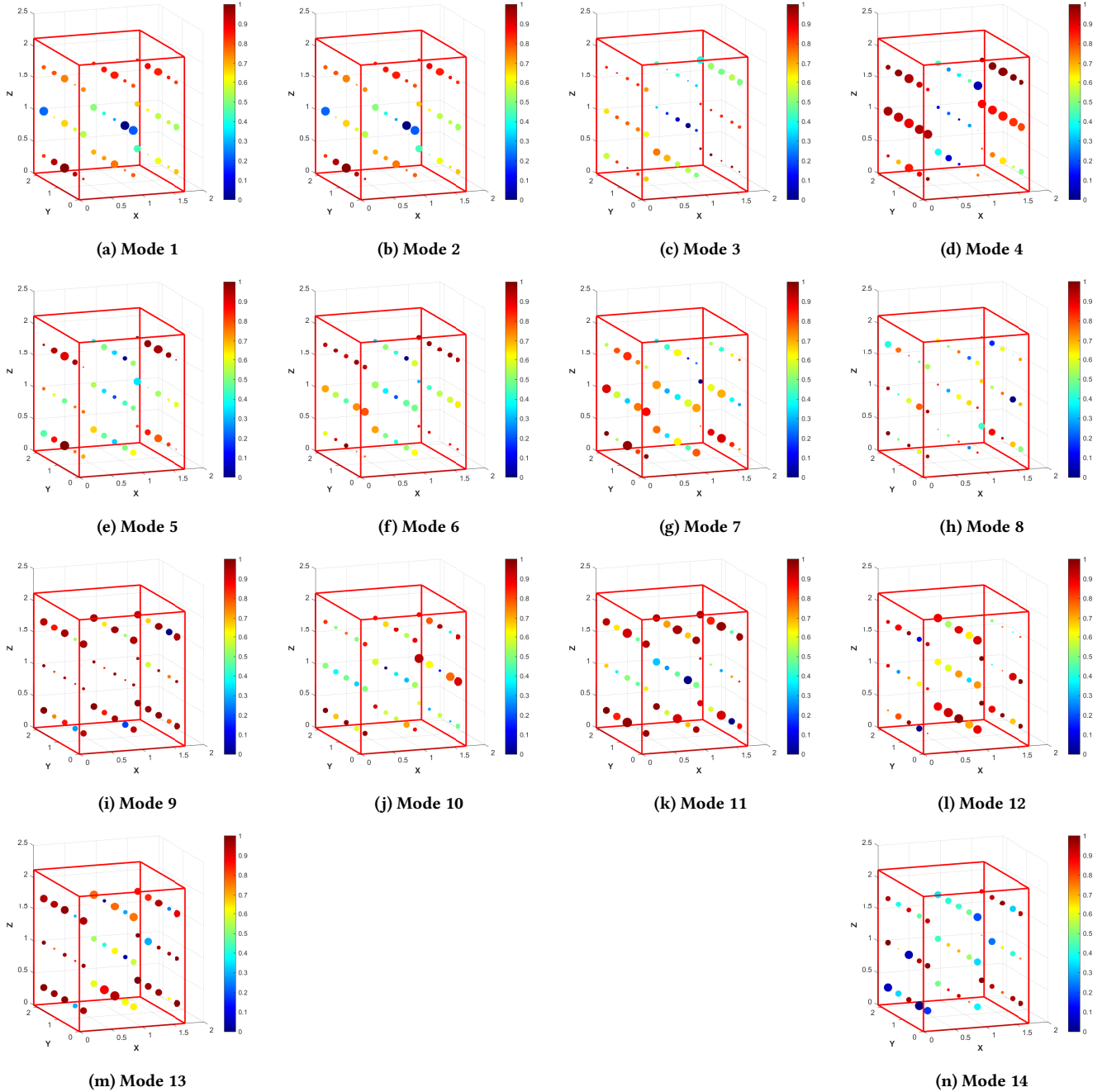


Figure 13: The recorded pressure values at 45 different locations in the room. The color of the point indicates pressure values, while the size indicates the error between recorded and simulation values.

Figure 6 shows that in some cases participants were facing opposite sides during the two experimental locations. This occurred for 5 modes; modes 2, 5, 7, 12, and 14. The distribution patterns for each location of these modes are separately provided in the appendix in Fig. 14. In most of these modes, the orientation of the participant did not have a significant effect on the location of sensations on the body.

B.1 Uniform vertical pressure modes

The modes considered in this subsection are the ones where the pressure distribution is even in the vertical direction (from head to toe), i.e., modes 1, 3, 5, 8, 12, and 14.

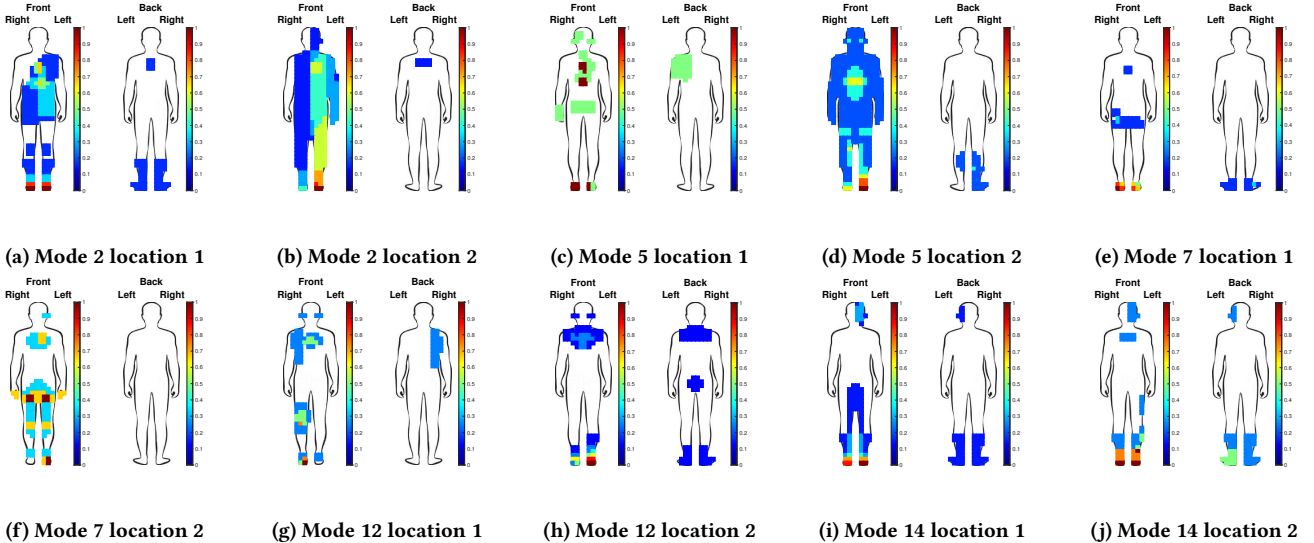


Figure 14: The Sensation distribution on different parts of the body for the five modes where participants were facing opposite sides for the two experimental locations. Each subfigure displays two silhouettes, one for the front of the body and one for the backside.

For modes 1, 5, and 8, the sensations were dispersed across various body regions, with particular emphasis on the chest, waist, and feet. Nonetheless, the distribution was expansive, covering the entire body.

Conversely, in modes 3 and 14, the visualizations suggest an intriguing phenomenon: although the pressure fields were vertically consistent, they lacked horizontal uniformity across the participant's body (see Fig. 6). This discrepancy appears to have a significant impact on the sensation locations reported. Specifically, sensations were predominantly marked around the feet and were partially distributed around the upper trunk and head regions. This pattern becomes even more noteworthy when considering that in modes 3 and 14, sensations were primarily felt on the right side of the head, which corresponds to the region of higher pressure.

Mode 12 presents a deviation from the expected sensation pattern observed in modes 1, 5, and 8. Despite sharing a similar vertical pressure distribution, sensations reported for mode 12 were predominantly focused around the feet and the outer upper chest area, conspicuously bypassing the mid-region of the body. This unusual distribution of sensation could potentially be attributed to the higher frequency associated with mode 12 or may indicate an emergent property that has yet to be identified.

B.2 Horizontally segmented dual pressure modes

This section focuses on the modes characterized by two horizontal slices of high pressure at the top and bottom, with pressure gradually diminishing towards the center. These modes include modes 2, 4, 6, 7, and 10.

For modes 6, 7, and 10, it is evident from Figure 12 that participants primarily reported sensations in the lower body and upper trunk regions. These observations align well with the simulated pressure patterns, making the outcomes anticipated.

Conversely, modes 2 and 4 exhibit a more expansive area of sensation, diverging from the expected patterns based on simulations. This discrepancy is likely attributable to the emergent properties which will be discussed in Section 8.3. It highlights that the lower frequency modes are perceived within the trunk area. While these sensations may not strictly align with the simulations, their presence indicates that factors other than just pressure fields are influencing the sensory experience.

B.3 Horizontally segmented tri-zonal pressure modes

Next, we turn our attention to the modes featuring three distinct horizontal pressure zones within the experimental regions, specifically Modes 9, 11, and 13.

Initially, it was hypothesized that these modes would behave similarly to those with uniform pressure distribution. The data, as illustrated in Fig. 12, largely corroborates this expectation. In fact, Modes 9 and 13 surpass expectations by clearly delineating three distinct sensation zones on the body. This outcome is particularly noteworthy because it can be challenging for human participants to precisely localize such sensations. It also demonstrates that the focusing capability of modes is significantly better at higher frequencies.

Mode 11 exhibits sensations dispersed across the entire body, with intermediate concentrations of higher sensation in the chest, waist, and lower leg areas. However, the sensation zones in mode 11 are not as clearly defined as those in Modes 9 and 13.